DETERMINING INTRUDER AIRCRAFT POSITION USING SERIES OF STEREOSCOPIC 2-D IMAGES

by

ADITYA RAMANI

Presented to the Faculty of the Graduate School of
The University of Texas at Arlington in Partial Fulfillment
of the Requirements
for the Degree of

MASTERS IN AEROSPACE ENGINEERING

THE UNIVERSITY OF TEXAS AT ARLINGTON

May 2016

Dedicated to my family and friends, especially my mother, Viji.

ACKNOWLEDGEMENTS

First, I would like to thank Dr. Atilla Dogan, my supervising professor, for his continuous guidance, encouragement, and support over the course of my research at The University of Texas at Arlington. Over the course of my research, Dr. Dogan has taught me innovative problem solving techniques which helped me in my thesis work in profound ways, in addition to answering all my inquiries with utmost patience and care. Additionally, in the capacity of graduate advisor, he helped guide me in picking a wide variety of courses, which in turn help expand my horizons to the various possibilities with which the concepts taught in class could be applied in the real-world. I consider myself lucky not only for the opportunity to work under him, but also for helping shape my life experiences in ways that allow me to gain the courage needed to face the real-world challenges.

I convey my special regards to Dr. Huff, Dr. Mullins, and Dr. Bowling for taking the time to be part of my thesis committee. In particular, I would like to thank Dr. Mullins, whose Flight Mechanics course provided me with all the tools necessary to complete my thesis research.

Lastly, I want to thank my friends and family, especially my mother, Viji. I certainly would not be where I am today if it weren't for her love, support, and encouragement.

May 4, 2016

ABSTRACT

DETERMINING INTRUDER AIRCRAFT POSITION USING SERIES OF STEREOSCOPIC 2-D IMAGES

Aditya Ramani, M.S.

The University of Texas at Arlington, 2016

Supervising Professors: Dr. Atilla Dogan

Introduction of UAV (Unmanned Aerial Vehicles) into the NAS (National Air Space) requires the detect-and-avoid capability. That is, an aircraft should be able to detect other aircraft flying in the same airspace volume and make evasive maneuvers if there is potential conflict. One potential methods currently investigated for detection of an intruder aircraft is to process digital images taken by onboard cameras. When and if intruder aircraft detection is successful through image processing, avoidance algorithms can greatly benefit from the relative position information. This thesis research investigates methods to compute the position of an intruder aircraft relative to an observer aircraft with onboard stereo cameras. To focus on relative position estimation rather than the intruder aircraft detection through image processing, the first phase of the research effort was to generate camera images given the relative position information. This process uses a simple pinhole camera methods where cameras are characterized by focal length, angle of view and resolution. The second phase of the research developed two methods to estimate the relative position based on the generated camera images. Both methods employ epipolar geometry of stereo

vision based on two cameras placed on the aircraft with lateral separation. Various cases are run in a Matlab/Simulink-simulation environment that is developed for this research. Simulation cases are designed to evaluate the relative position estimation methods with different aircraft trajectories, different camera separation, and different camera resolution. Simulation results show that relative position can be estimated while both aircraft are flying along any trajectories as long as the intruder aircraft is visible by both cameras. The estimation accuracy degrades as the relative distance increases between the aircraft. The larger lateral separation seems to improve the estimation accuracy. Image resolution seems to have little to no impact on estimation accuracy.

TABLE OF CONTENTS

LIST OF FIGURES

CHAPTER 1

Introduction

This chapter introduces the research problem solved in the research effort. This task is accomplished by first explaining the problem statement for the thesis research, followed by describing its real-world applications, before finally giving a brief overview of the thesis' organization.

1.1 Research Motivation

There is an increasing demand for UAS to operate in the NAS (National Air Space). This requires UAS to have the detect-and-avoid capability, i.e., UAS sharing the air space with piloted aircraft and other unmanned aircraft should be able to detect any incoming aircraft, evaluate the probability of conflict, and maneuver to resolve the conflict. Some of the ways with which this is accomplished now include ADS-B (Automatic dependent Surveillance-Broadcast), which uses GPS technology to determine aircraft location and speed data [1]. However, some aircraft may note be equipped with ADS-B, due to which one of the most effective methods for which one can detect an intruder aircraft is to use camera images [2], which does not have any restriction on the type of aircraft that can be detected as long as its within the field of view of the cameras.

Another area where the determination of aircraft position could be useful is in the area of surveillance, where UAS can also be used to detect and track any aircraft unwelcome in a particular airspace and determine not only the type of aircraft (such

as military or civilian), but also whether the aircraft had deviated from its flight path or not, intentionally or unintentionally.

1.2 Thesis Objective

The position of an aircraft is defined in 3-dimensions (i.e.,in the x, y, and z directions). If one wants to determine the position of an aircraft using photographic images, a single 2-dimensional photograph will not help in determining the location of an aircraft due to the fact that in order to determine a 3-D position, depth perception is absolutely essential to finding the desired answer. The only way with which this can be achieved is if one has not one, but at least 2 2-D images taken not only at exactly the same instances, but also have the cameras (taking each of the images) some distance apart. One of the ways with which one can take multiple 2-D images at the same instance would be through a stereoscopic camera, which works in a similar fashion as the human eye in that each eye (or one of the 2 cameras in the case of a stereoscopic camera) observes a 2-dimensional space and two eyes (when working together) combine the two 2-dimensional space and perceive a single 3-dimensional space. This, in turn, allows one to determine the location of an object in space at a much higher accuracy than one would with just a single eye. Extending this concept to a stereoscopic camera, one can determine the exact position of any object in space. **The main objective of this research is to develop an effective method with which one can determine the 3-dimensional position of an intruder aircraft relative to the observer aircraft by using a series of stereoscopic images taken from the latter aircraft.**

In order to focus on relative position estimation, rather than image processing to identify whether an intruder aircraft is visible, and if so, where it is on camera frames, the camera images are also generated artificially in simulation. With this

approach, the following steps are taken to accomplish the research objective stated above.

1. Given the position and orientation of each aircraft relative to the common inertial frame, formulate the position of the intruder aircraft relative to the observer aircraft, expressed in the observer's body frame.
2. Given the position and orientation of each camera, formulate the position of intruder aircraft relative to each camera, expressed in the camera frame.
3. Given the angle of view and resolution of the camera in each direction, generate a matrix with all zeros, except 1 at the position where the intruder aircraft would be seen, only if the intruder aircraft is within the camera's field of view. This matrix simulates the result of an image processing algorithm that detects the intruder aircraft and puts 1 at the corresponding cell while all the other cells of the matrix are set to zero.
4. Using the generated camera images from two cameras, formulate the position estimation of the intruder aircraft relative to the observer aircraft body frame.
5. Define and simulate various cases with different aircraft trajectory.
6. Compare the actual relative position of the intruder aircraft with the estimated relative position based on camera images.

1.3 Thesis Organization and Contribution

1.3.1 Thesis Organization

This section explains the overall organization of the thesis, providing a brief summary of what each chapter discusses.

Chapter 1 introduces the reader to the topic, mentioning the problem statement and ita real-world applications.

Chapter 2 focuses on camera image generation, defining and simulating several different test cases to demonstrate the process.

Chapter 3 formulates the position estimation of the intruder aircraft relative to the observer aircraft body frame using the generated camera images From Chapter 2, revising its test cases and comparing the results obtained.

Chapter 4 concludes the document by providing an overall summary of the final results obtained and the conclusions reached. It also describes future work that can be done to improve upon the results obtained and its real-world applications.

1.3.2 Contribution

The main contribution of this research work to develop an effective method with which one can determine position of an object using images. This research effort is unique in that it eliminates image processing techniques and uses in its place two-dimensional binary matrices to simulate intruder aircraft images taken from an observer aircraft.

CHAPTER 2

Camera Image Generation

The overall focus of this chapter is to explain how to generate camera image(s) of an intruder aircraft relative to an observer aircraft. This is accomplished in two steps: the first is developing a method with which a flight can be simulated where one can determine the position of an intruder aircraft relative to an observer aircraft; and the second is taking the resulting position values and essentially 'transferring' them to cameras located at predetermined locations on the observer aircraft. In both cases, the equations used will be explained in detail, as well as providing the reader with occasional pictorial illustrations of how such an algorithm is implemented.

2.1 Reference Frames and Rotation Matrices

The inertial frame is defined to be a frame of reference that describes time and space in a homogeneous, isotropic, and time-independent manner. This frame is defined to have its origin at a geometrically fixed point in space and the axes are defined as follows:

- The positive x-axis points along local north
- The positive y-axis points along local east
- The positive z-axis points along local down

This frame is referred to as I-frame in the rest of the thesis.

The body-fixed frame of Aircraft i is defined to have its origin at a geometrically fixed position in the aircraft (in this case the aircraft's Center of Gravity (COG)) and the axes, as shown in Fig. 2.1, are defined as follows:

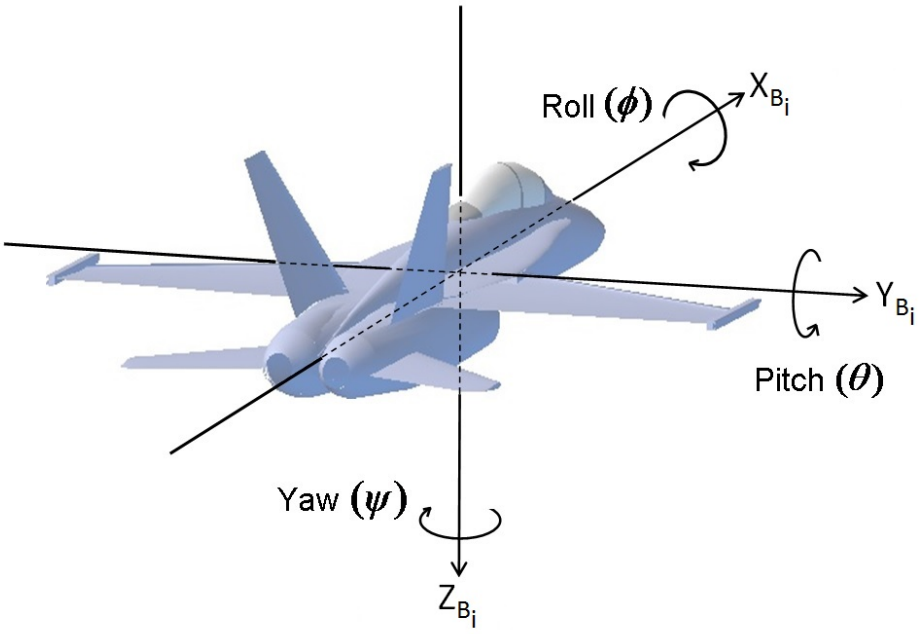

Figure 2.1. Body-Fixed Frame of Aircraft i.

- The positive x-axis points along the fuselage toward the nose of the aircraft (local north)
- The positive y-axis points to the right of the aircraft (local east)
- The positive z-axis points downward in a manner that the x-z plane is both orthogonal to the x-y frame and travels along an aircraft's plane of symmetry (local down)

This frame is referred to as B_i-frame in the rest of the thesis.

The wind frame of Aircraft i is defined in a manner that describes the aerodynamic forces acting on an aircraft. It is defined to have its origin at the same geometrically fixed point in the aircraft as the B_i-frame and have the same axes def-

inition as the latter frame. they are characterized by the angle of attack, α, and the angle of side-slip, β. This frame is referred to as W_i-frame in the rest of the thesis.

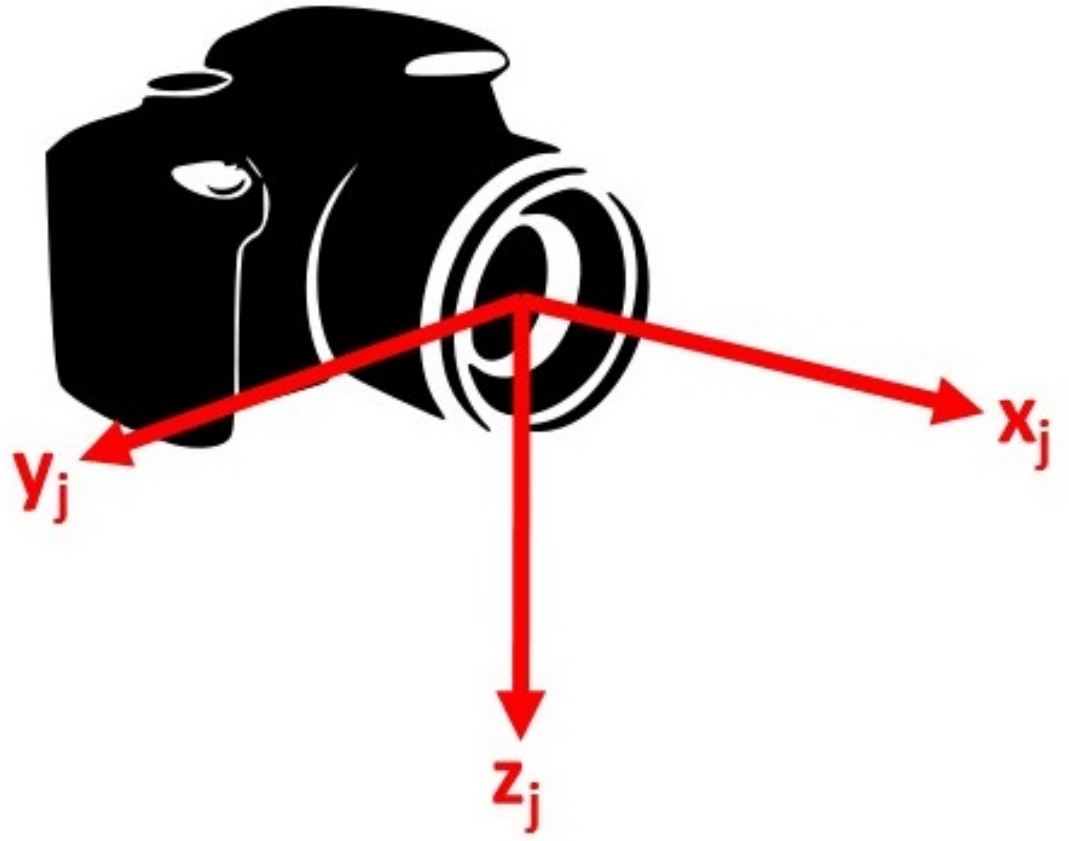

Figure 2.2. XYZ Frame - Camera-j.

The camera-j frame is defined to have its origin at the center of the camera lens, and x-axis pointing along the normal line of view, as depicted in Fig. 2.2. This frame is referred to as C_j-frame, where j indicating camera-j on the aircraft.

To write a vector in terms of its components in the specified frame, vectrix formulation will be employed. This facilitates two things at once:

- it allows the expression of a vector in terms of its representation in a frame
- it allows one to transform the representation of a vector to another frame using the corresponding rotation matrix [3]

In order to rotate from one frame to another, rotation matrices must be used. The rotation matrices used for this thesis include:

- $\mathbf{R_{C_jB_i}}$, which is the rotation matrix used to rotate from the C_j-frame to the B_i-frame
- $\mathbf{R_{B_iI}}$, which is the rotation matrix used to rotate from the I-frame to the B_i-frame
- $\mathbf{R_{B_iW_i}}$, which is the rotation matrix used to rotate from the W_i-frame to the B_i-frame

The vectrix of B_i-frame is denoted by $[\hat{\underline{B}}_i]$ and the relationship between the vectrices of the I-frame and B_i-frame is established through the rotation matrix from I-frame to B_i-frame as:

$$[\hat{\underline{B}}_i] = \mathbf{R_{B_iI}}[\hat{\underline{I}}] \tag{2.1}$$

Likewise, using orthonormality of rotation matrices, one can transform from the B_i-frame to the I-frame using the equation:

$$[\hat{\underline{I}}] = \mathbf{R_{B_iI}}^T[\hat{\underline{B}}_i] \tag{2.2}$$

The terms defined above serve as a foundation on which all the equations necessary to solve the thesis problem statement are built. The rest of this chapter will focus on generating the camera images, while the subsequent chapter will focus on extracting the intruder aircraft position using the generated images.

2.2 Formulation

2.2.1 Determining 3-D Position of Intruder Aircraft

Consider Aircraft 1 to be the observer aircraft (which is equipped with the cameras) and Aircraft 2 to be the intruder aircraft. The goal of this step is to express the position of Aircraft 2 with respect to Aircraft 1. First, the representation of velocity of each aircraft in inertial frame is written in terms of airspeed V, using the translational kinematics equation:

$$\dot{r}_{B_i} = \mathbf{R}_{B_iI}^T \mathbf{R}_{B_iW_i} U \tag{2.3}$$

where $i = \{1, 2\}$ and $U = [V\ 0\ 0]^T$. In addition to these equations, the rotational kinematics equations are also used, expressed in terms of angles ψ , θ and ϕ and pitch, roll, and yaw rates p, q, and r, as shown below:

$$\dot{\psi} = (q \sin\phi + r \cos\phi) \sec\theta \tag{2.4}$$

$$\dot{\theta} = q \cos\theta - r \sin\theta \tag{2.5}$$

$$\dot{\phi} = p + q \sin\phi \tan\theta + r \cos\phi \tan\theta \tag{2.6}$$

These equations are then implemented in Simulink. Note that the input to the aircraft equations in Simulink are: the aircraft speed, the angles β and α (which represent the rotation of the aircraft between the aircraft body frame and the aircraft wind frame), and p, q, and r; all of these variables are specified in advance prior to running the simulation.

As depicted in Fig. 2.3, the relative position of Aircraft 2 with respect to Aircraft 1 can be expressed in terms of the position vector of each aircraft with respect to the I-frame as:

$$\underline{\xi} = \underline{r}_{B_2} - \underline{r}_{B_1} \tag{2.7}$$

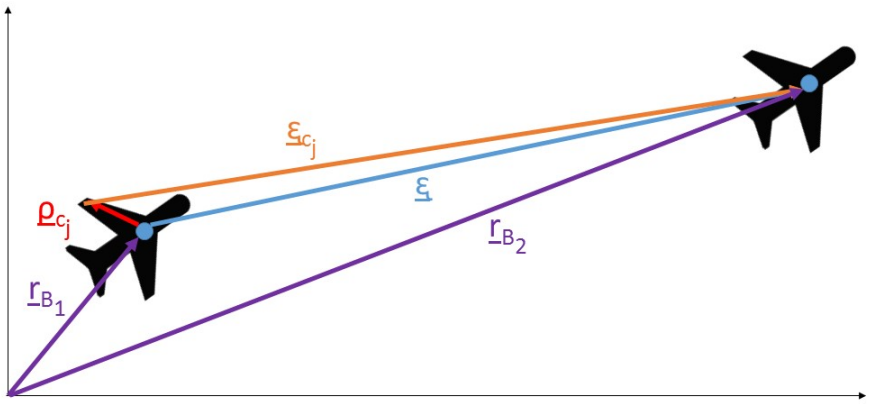

Figure 2.3. Position of the 2 Aircraft and Camera j relative to inertial frame.

Defining ξ, the representation of the relative position vector in the B_1-frame, and r_{B_1} and r_{B_2}, the representations of the position vectors of the two aircraft in the I-frame, the vectors can be expressed as:

$$\underline{\xi} = [\underline{\hat{B}_1}]^T \xi$$

$$\underline{r}_{B_1} = [\underline{\hat{I}}]^T r_{B_1}$$

$$\underline{r}_{B_2} = [\underline{\hat{I}}]^T r_{B_2}$$

Substituting these relations in Eq. (2.7) and using the vectrix relations in Eq. (2.1) lead to:

$$\begin{aligned} \underline{\xi} &= [\underline{\hat{I}}]^T r_{B_2} - [I]^T r_{B_1} \\ [\underline{\hat{B}_1}]^T \xi &= [\underline{\hat{I}}]^T (r_{B_2} - r_{B_1}) \\ \mathbf{R_{B_1 I}^T} \xi &= (r_{B_2} - r_{B_1}) \\ \xi &= \mathbf{R_{B_1 I}} (r_{B_2} - r_{B_1}) \end{aligned} \tag{2.8}$$

which gives the representation of Aircraft 2 position relative to Aircraft 1 in B_1-frame in terms of representations of Aircraft 1 and 2 positions in the the I-frame.

2.2.2 Transferring Relative Position to Images

Once the position of the intruder aircraft (Aircraft 2) relative to the B_1-frame with cameras (Aircraft 1), is formulated in B_1-frame, the next step is to formulate the Aircraft 2 position relative to each camera placed at a specified position and with a specified orientation relative to the B_1-frame. This relative position vector with respect to each camera should be expressed in the C_j-frame to facilitate the generation of camera images.

As depicted in Fig. 2.4, $\underline{\rho}_{C_j}$ is the position vector of camera-j and $\underline{\xi}_{C_j}$ is the position vector of Aircraft 2 relative to Aircraft 1's C_j-frame. Let ρ_{C_j} be the representation of $\underline{\rho}_{C_j}$ in B_1-frame and ξ_{C_j} be the representation of $\underline{\xi}_{C_j}$ in C_j-frame. Using the vector relations and the rotation matrix from B_1-frame to C_j-frame, $R_{C_j B_1}$, representation ξ_{C_j} can be calculated as:

$$\xi_{C_j} = R_{C_j B_1} (\xi - \rho_{C_j}) \tag{2.9}$$

Given the position of the intruder aircraft relative to the camera, expressed in C_j-frame, the next step is to formulate the projection of the intruder aircraft position

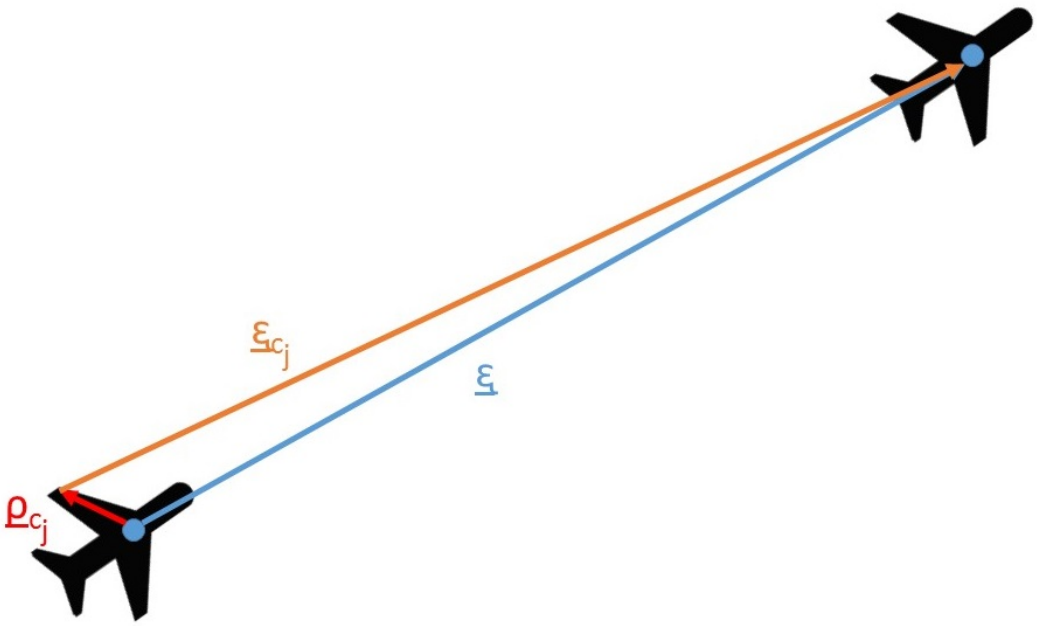

Figure 2.4. Position ρ_{C_j} on Observer Aircraft.

on the image plane of the camera. This is used to generate the camera image, after it is image-processed and the aircraft image is identified, if it is in the Field of View (FOV). The pinhole camera model approach is employed to complete this task, in this ideal pinhole camera model, the camera aperture is considered to be a point, and no lenses are used to focus light [4]. The output of this procedure will be a 2-D matrix, representing the processed image file from a digital camera. The size of the matrix quantifies the resolution of the camera. The other two camera parameters considered are angle of view (γ_{z_j}) and the focal length (f_{C_j}), depicted in Fig. 2.5. The length of the (virtual) image plane along the y_{C_j}-axis is $2l_{Cy_j}$ where

$$l_{Cy_j} = f_{C_j} tan\gamma_{z_j} \tag{2.10}$$

Similarly, in the (x_{C_j}, z_{C_j}) plane, the length of the (virtual) image plane along z_{C_j}-axis is $2l_{Cz_j}$ where

$$l_{Cz_j} = f_{C_j} tan\gamma_{y_j} \tag{2.11}$$

where γ_{y_j} is the angle of view in the (x_{C_j}, z_{C_j}) plane.

The projection of an object on the image plane, according to the pinhole model, is rotated by 180 degrees. To avoid working with an inverted image, the formulation in the following steps will be carried out on the virtual image plane, as shown in Fig. 2.5.

The (virtual) image plane is divided into a grid (see Fig. 2.6) that is corresponding to the image matrix this process will output. The sizes of the grid - and thus the image matrix $\mathbf{M}(i_{N_z}, i_{N_y})$ - is determined by the resolution of the digital image the camera records. The number of rows is N_{z_j} (the number of grid points, or pixels along the z_{C_j}-axis) and the number of columns is N_{y_j} (the number of grid points, or pixels along the y_{C_j}-axis). N_{y_j} and N_{z_j} are considered to be odd numbers. Indices i_{N_y} and i_{N_z} in $\mathbf{M}(i_{N_z}, i_{N_y})$ indicate the row and column numbers, respectively, or the location of the corresponding pixel on the image plane.

In this context, the questions become: (i) whether the intruder aircraft will be visible on the (virtual) image plane, given the relative position of the intruder aircraft with respect to the camera frame, and (ii) if visible, what the row and column numbers (i_{N_z}, i_{N_y}) of the image matrix will be for the projection of the intruder aircraft on the (virtual) image plane.

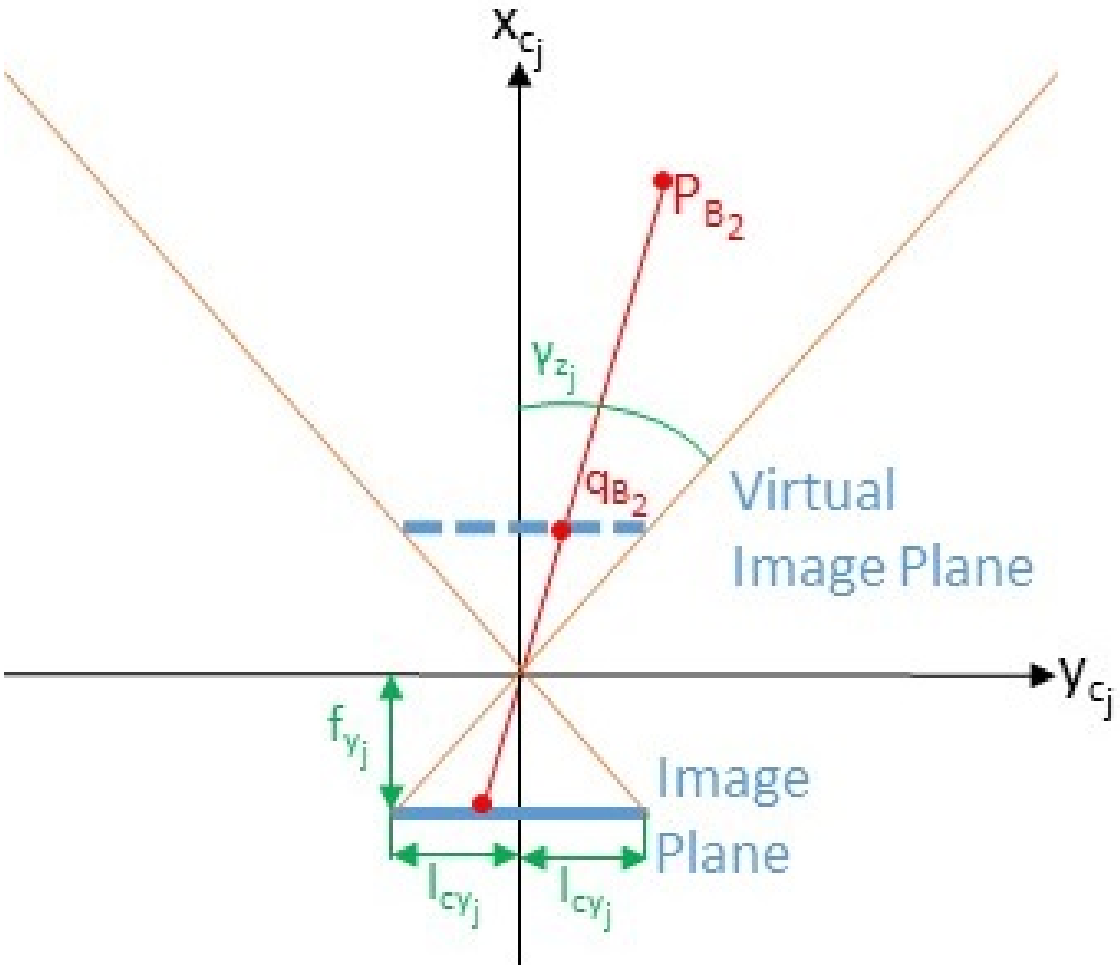

Figure 2.5. Pinhole camera model.

Consider point p_{B_2} in Fig. 2.5 representing Aircraft 2, which means the position of point p_{B_2} in C_j-frame is ξ_{C_j}, as formulated in Eq. (2.9). The three components of ξ_{C_j} in C_j-frame is:

$$\xi_{C_j} = \begin{bmatrix} \xi_{Cx_j} \\ \xi_{Cy_j} \\ \xi_{Cz_j} \end{bmatrix} \tag{2.12}$$

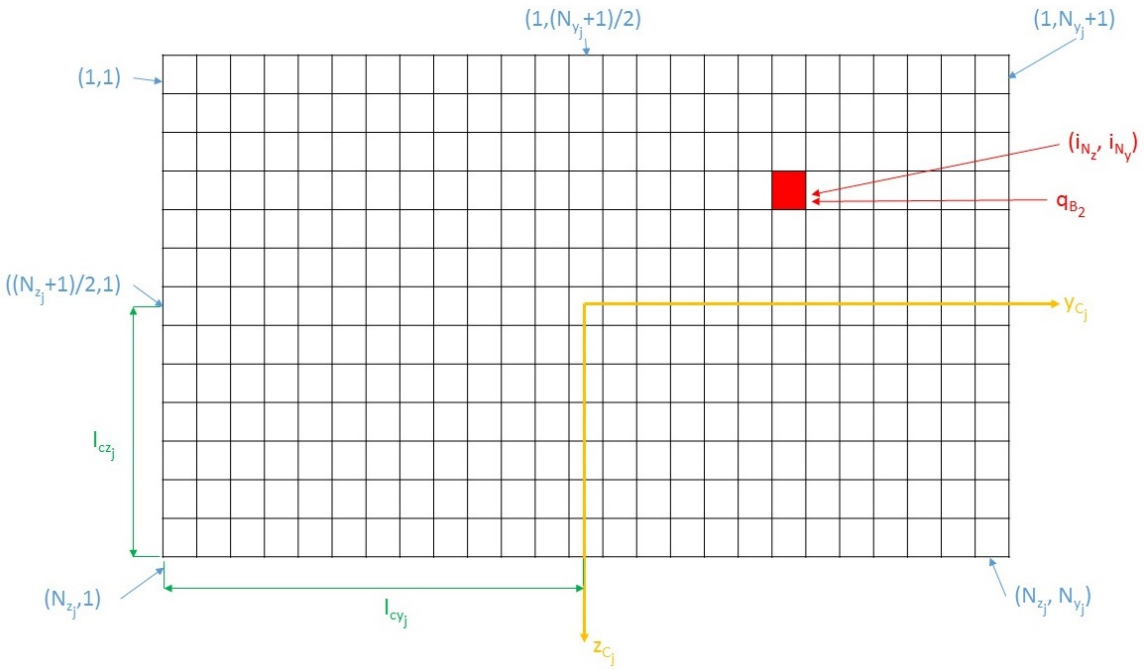

Figure 2.6. Virtual image frame and image matrix.

Consider point q_{B_2} to be the projection of point p_{B_2} on the virtual image plane, as shown in Figs. 2.5 and 2.6. The position of point q_{B_2} in C_j-frame is defined as:

$$\xi_{q_{B_2}} = \begin{bmatrix} f_{C_j} \\ y_{C_j} \\ z_{C_j} \end{bmatrix} \tag{2.13}$$

where f_{C_j} is the focal length.

Through the geometric relations, it can be shown that:

$$\frac{y_{C_j}}{f_{C_j}} = \frac{\xi_{Cy_j}}{\xi_{Cx_j}} \tag{2.14}$$

and

$$\frac{z_{C_j}}{f_{C_j}} = \frac{\xi_{Cz_j}}{\xi_{Cx_j}} \tag{2.15}$$

which imply

$$y_{C_j} = f_{C_j} \frac{\xi_{Cy_j}}{\xi_{Cx_j}} \tag{2.16}$$

$$z_{C_j} = f_{C_j} \frac{\xi_{Cz_j}}{\xi_{Cx_j}} \tag{2.17}$$

To quantify where point q_{B_2} is on the virtual image plane, two integer quantities are computed as:

$$i_y = int(100 \frac{y_{C_j}}{l_{y_{C_j}}}) \tag{2.18}$$

$$i_z = int(100 \frac{z_{C_j}}{l_{z_{C_j}}}) \tag{2.19}$$

where int is the integer operator that turns a real number to the closest integer, $l_{y_{C_j}}$ and $l_{z_{C_j}}$ are the length of the virtual image plane in y_{C_j} and z_{C_j}-axes respectively. Note that i_y and i_z vary from -100 to 100, when point q_{B_2} is within the (virtual) image frame. If $i_y \notin (-100, 100)$ or $i_z \notin (-100, 100)$, then point q_{B_2} is not within the (virtual) image frame, which occurs when the intruder aircraft is not within the FOV.

Integers i_y and i_z in Eqs. (2.18) and (2.19) can be expressed alternatively. Substituting $l_{y_{C_j}}$ and $l_{z_{C_j}}$ from Eqs. (2.10) and (2.11) respectively into Eqs. (2.18) and (2.19) yield:

$$i_y = int(100 \frac{\xi_{Cy_j}}{\xi_{Cx_j}} tan\gamma_{z_j}) \tag{2.20}$$

$$i_z = int(100 \frac{\xi_{Cz_j}}{\xi_{Cx_j}} tan\gamma_{y_j}) \tag{2.21}$$

In these formulation, the indices are calculated from the relative position coordinates of the intruder aircraft in C_j-frame and angles of view of the camera. Note that these formulations do not require the focal length as they use the angle of view instead.

The last step is to compute the indices for the row and column numbers of the image matrix. This can easily be shown to be:

$$i_{N_y} = \frac{N_{y_j} - 1}{2}(\frac{i_y}{100} + 1) + 1 \tag{2.22}$$

$$i_{N_z} = \frac{N_{z_j} - 1}{2}(\frac{i_z}{100} + 1) + 1 \tag{2.23}$$

where i_{N_y} and i_{N_z} vary between 1 and N_{y_j} and N_{z_j} respectively when q_{B_2} is within the (virtual) image frame. When q_{B_2} is at the upper left corner, $i_{N_y} = i_{N_z} = 1$. When q_{B_2} is at the lower right corner, $i_{N_y} = N_{y_j}$ and $i_{N_z} = N_{z_j}$. In other words, when q_{B_2} is inside the (virtual) image frame, i.e., when the intruder aircraft is within the FOV:

$$1 \leq i_{N_y} \leq N_{y_j} \tag{2.24}$$

$$1 \leq i_{N_z} \leq N_{z_j} \tag{2.25}$$

Otherwise, the intruder aircraft should be outside the FOV. When the intruder aircraft is within the FOV, i.e., the conditions in Eqs. (2.24) and (2.25) are met, the image matrix, whose size is $N_{z_j} \times N_{y_j}$, and is initialized to be $M(i,j) = 0_{N_{z_j} \times N_{y_j}}$, is modified as:

$$\mathbf{M}(i_{N_z}, i_{N_y}) = 1 \tag{2.26}$$

This means the whole image matrix is zero, except the row i_{N_z} and i_{N_y} is 1, indicating the pixel corresponding to appearance of the intruder aircraft in camera image.

2.3 Simulation Results

This section discusses four cases used to simulate the above equations in order to verify the veracity of the theory. All cases have a few parameters in common:

- A total of two cameras are used for each case.
- The angle of attack and side-slip angles (α and β respectively) used are $[0 \;\; 0]^T$ for both Aircraft 1 and Aircraft 2 for each case.

- The angle of view γ_{z_j} is equal to 60 deg (or $\frac{\pi}{3}$ radians) for each camera.
- The two cameras are aligned such that there is no rotation relative to each other and the B_1-frame. As a result, the rotation matrix $R_{C_jB_1}(j = \{1, 2\})$ is the identity matrix I for all cameras.
- Unless otherwise noted, the two cameras use the same position parameters as the flight experiment conducted by NASA. In this case, the location parameters are: $\rho_{C_1} = [3\frac{3}{16}''\ \ 34\frac{19}{32}''\ \ 0'']^T$ and $\rho_{C_2} = [3\frac{3}{16}''\ \ -34\frac{19}{32}''\ \ 0'']^T$, respectively.
- All simulation cases run for a total time of 10 seconds.
- Unless otherwise noted, N_y and N_z (i.e. number of pixels along y and z axis respectively) are 3839 and 2159 respectively for all camera-j's. This means that focal length is: $f_{C_j} = \frac{N_{y_j} - 1}{2}\frac{1}{tan\gamma_{z_j}} = 1107.94$. (See Chapter 3 and [5] for equation derivation).
- The resulting images show Aircraft 2 at the first five time instances in which they are visible at each camera. Unless otherwise noted, the interval between each time instance is 0.1 second.

2.3.1 Case 1

The first case involves the following parameters/initialization values:

- Aircraft 1 is located at the origin of I-frame ($[0\ \ 0\ \ 0]^T$) and Aircraft 2 is located at $[0\ \ 3\ \ 0]^T$.
- Aircraft 1 and 2 travel at the speed of 100 m/s and 105 m/s, respectively.
- Both aircraft travel along a straight path (i.e. Euler angles are $[0\ \ 0\ \ 0]^T$).

The paths of the two aircraft during the simulation and the relative position of Aircraft 2 with respect to Aircraft 1 in terms of the three components in B_1-frame are shown

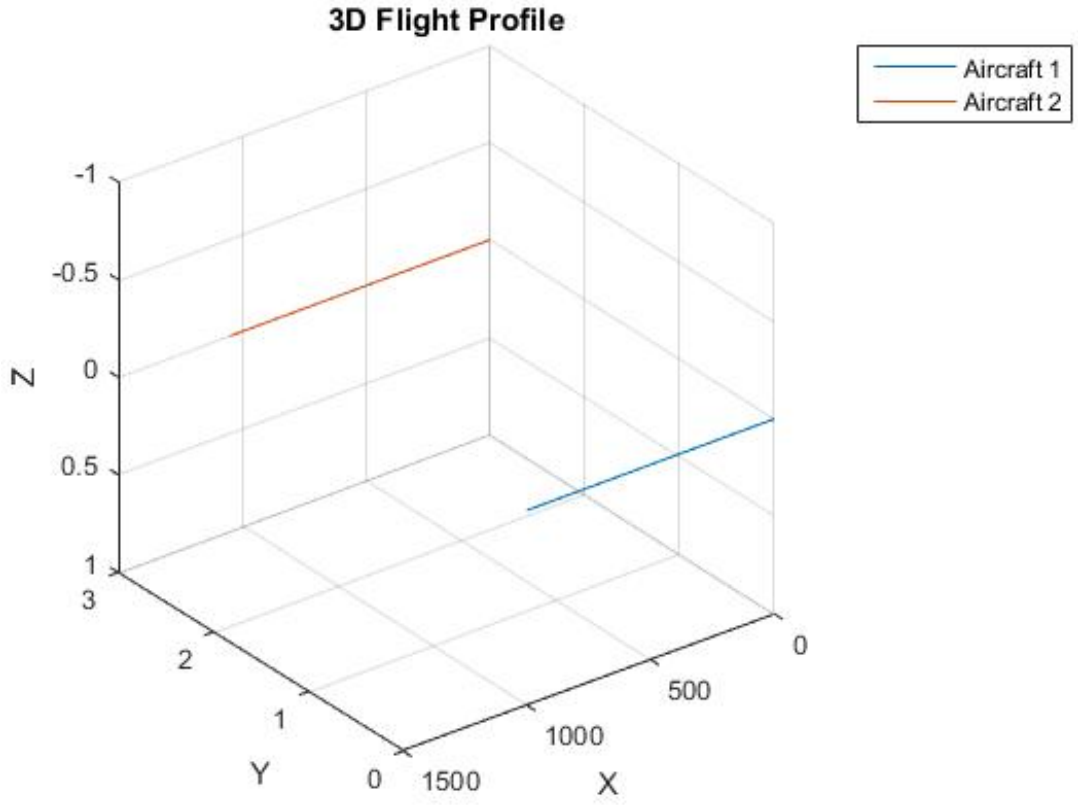

Figure 2.7. Case 1: 3D Flight Profile.

in Figs. 2.7 and 2.8, respectively. The resulting camera images procured of Aircraft 2 in their respective C_j-frame are shown in Figs. 2.9 and 2.10.

From the figures, one can clearly see that the distance between the aircraft image points are steadily decreasing along the center of the image, indicating that the aircraft is moving at a straight line parallel to and away from the observer aircraft over time. Additionally, the aircraft shows up on the right camera earlier than the left camera. This, in turn, proves that the camera image generation algorithm works as anticipated in this case.

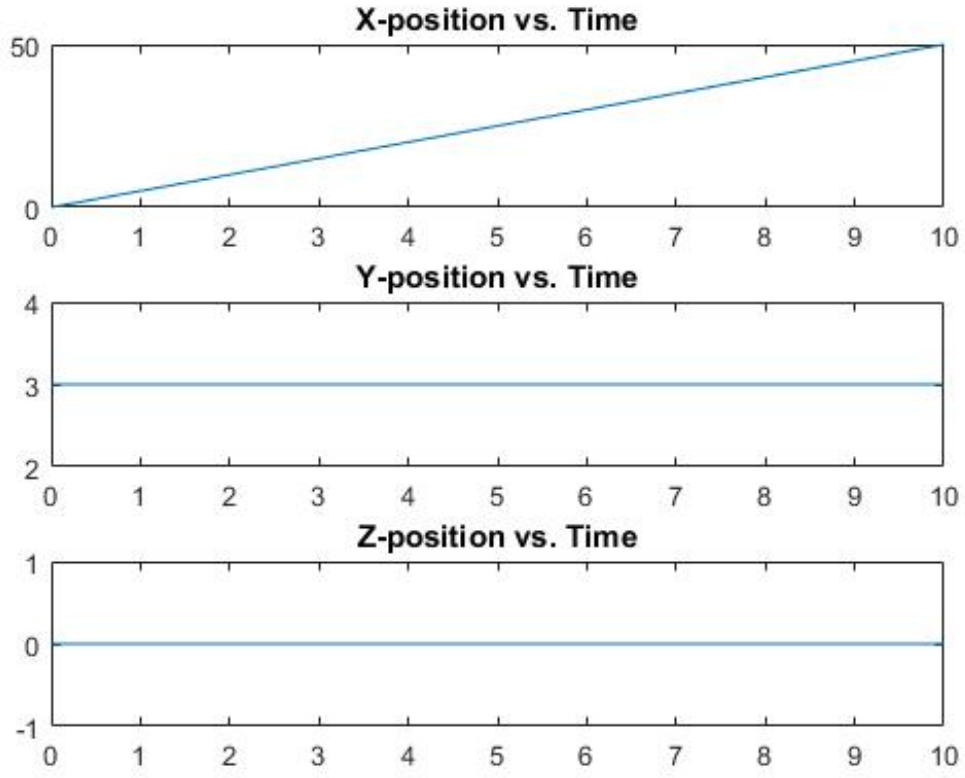

Figure 2.8. Case 1: B_1-frame components of Aircraft 2 w.r.t Aircraft 1.

2.3.2 Case 2

In this case, the initial positions, the speeds, and simulation time are the same as in Case 1, above. Yaw and pitch angles of Aircraft 2 are set to -1 and 1 deg, respectively. Figs. 2.11 and 2.12 show the paths of the two aircraft during the simulation and the relative position of Aircraft 2 with respect to Aircraft 1 in terms of the three components in B_1-frame. The location of the aircraft at each interval relative both cameras in their respective C_j-frame are shown in Figs. 2.13 and 2.14, respectively. Based on the images, it can be observed that not only are the points spaced much more closely together on the right camera than the left camera (indicating that the

Figure 2.9. Case 1: Intruder Aircraft Right Camera Image.

Figure 2.10. Case 1: Intruder Aircraft Left Camera Image.

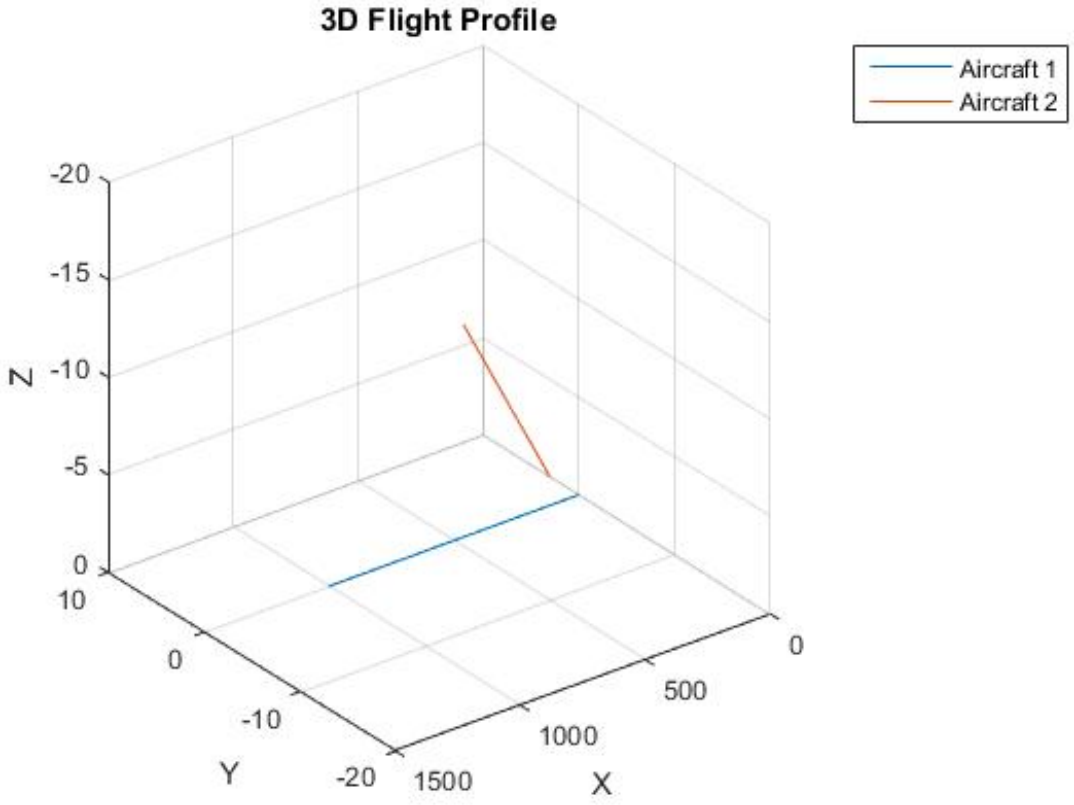

Figure 2.11. Case 2: 3D Flight Profile.

aircraft is closer to the left camera than the right as the wider the gap between points, the closer it is), but like Case 1, the aircraft is visible on the right camera earlier than the left camera.

2.3.3 Case 3

In this case, the speeds and simulation time are the same as in Cases 1 and 2, above. The initial position of Aircraft 2 for this case is $[600 \quad -300 \quad 0]^T$, while the initial yaw angle is 90 deg (i.e., Aircraft 2 is flying steadily in a direction perpendicular to Aircraft 1). Figs. 2.15 and 2.16 show the paths of the two aircraft during the

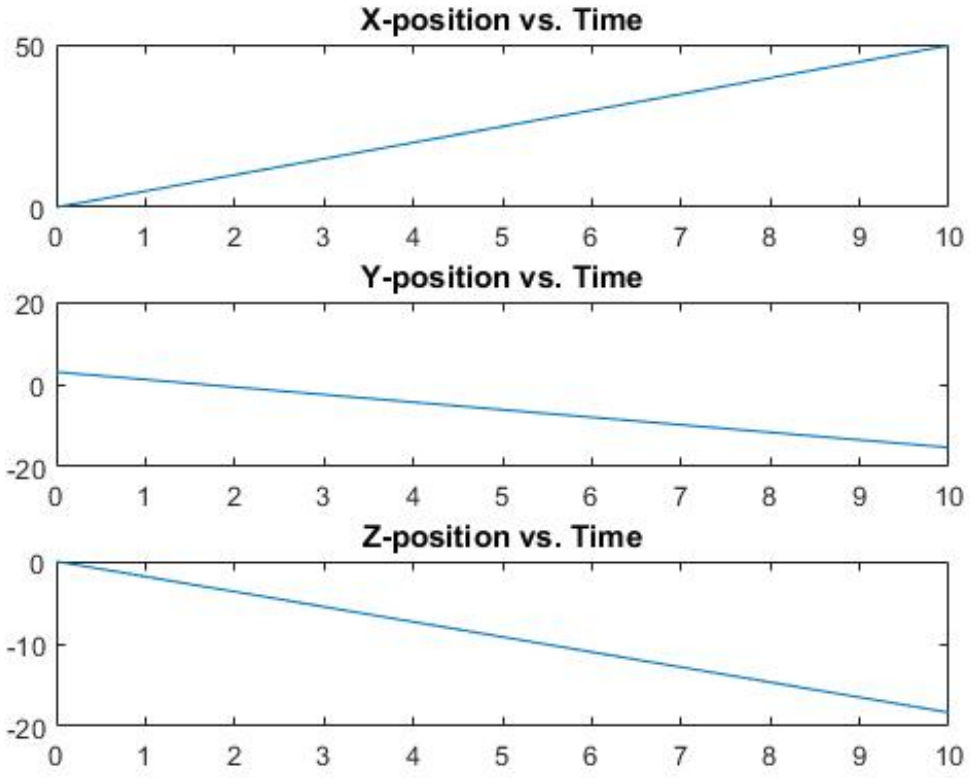

Figure 2.12. Case 2: B_1-frame components of Aircraft 2 w.r.t Aircraft 1.

simulation and the relative position of Aircraft 2 with respect to Aircraft 1 in terms of the three components in B_1-frame. The location of the aircraft at each 1-second interval relative both cameras in their respective C_j-frame are shown in Figs. 2.17 and 2.18, respectively. In this case, it can be observed that the intruder aircraft (Aircraft 2) simply flies perpendicular and eastward relative to Aircraft 1, and consequently, the aircraft is only visible for a short duration of the simulation (approximately the first 4 seconds).

Figure 2.13. Case 2: Intruder Aircraft Right Camera Image.

Figure 2.14. Case 2: Intruder Aircraft Left Camera Image.

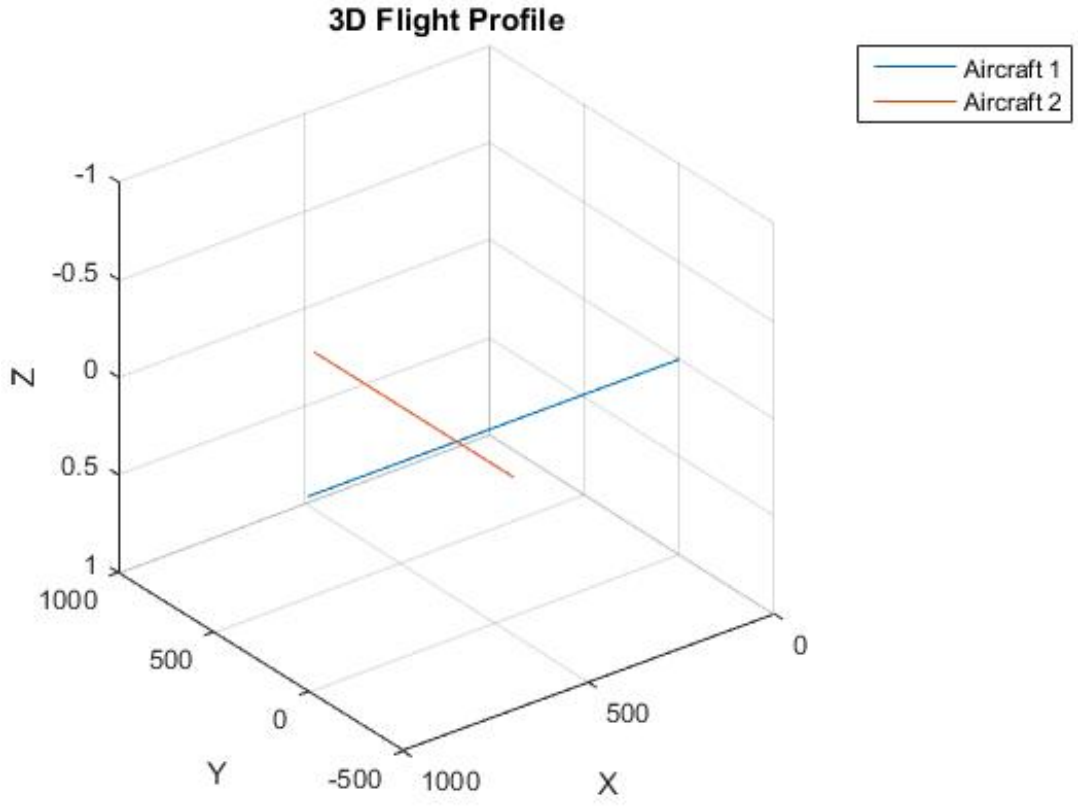

Figure 2.15. Case 3: 3D Flight Profile.

2.3.4 Case 4

This case is a repeat of Case 1, but with increased distance between the cameras. The previous cases all used the camera parameters used in the NASA project. This case will place the cameras such that each camera is placed 1.5 m along the left and right of the B_1-frame origin (i.e., $\rho_{C_1} = [3\frac{3}{16}''\quad 1.5m\quad 0'']^T$ and $\rho_{C_2} = [3\frac{3}{16}''\quad -1.5m\quad 0'']^T$ respectively). The paths of the two aircraft during the simulation and the relative position of Aircraft 2 with respect to Aircraft 1 in terms of the three components in B_1-frame are shown in Figs. 2.7 and 2.8, respectively. The location of the aircraft at each interval relative both cameras in their respective C_j-frame are

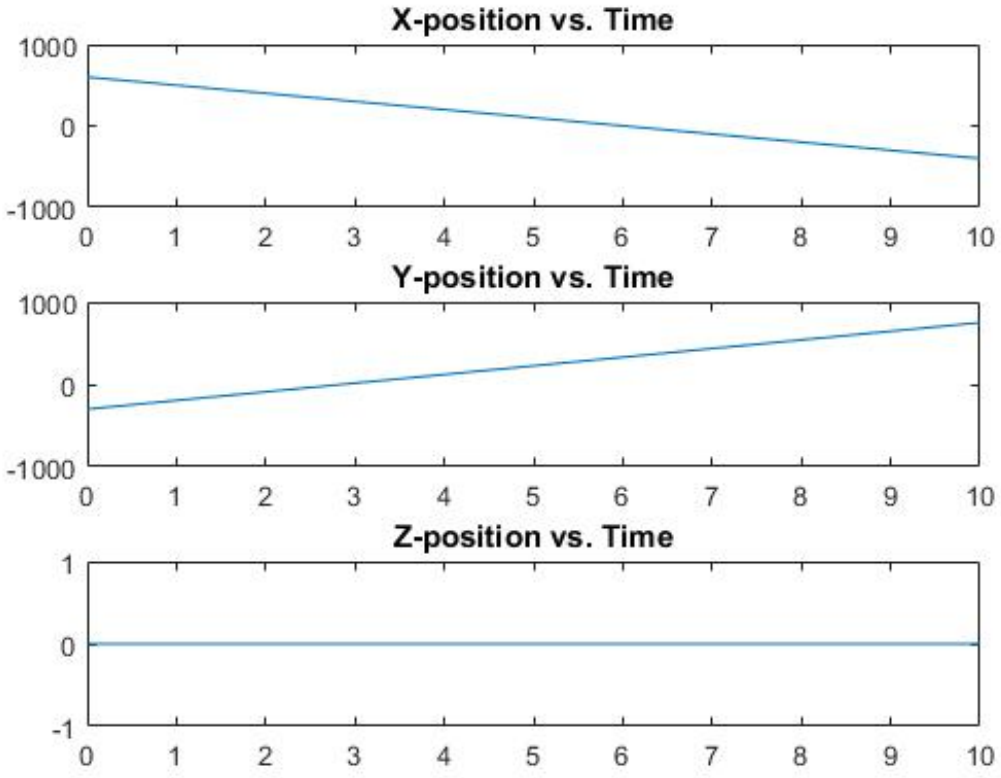

Figure 2.16. Case 3: B_1-frame components of Aircraft 2 w.r.t Aircraft 1.

shown in Figs. 2.19 and 2.20. As one can observe, the images are virtually identical to the ones procured in Case 1, but with clearly defined gaps in image points at each interval, especially on the right camera.

2.3.5 Case 5

This case is a repeat of Case 2, but with different image resolution. The values for N_y and N_z in this case will be 2001 and 1001 respectively, meaning that the focal length for this case will be: $f_{C_j} = \frac{N_{y_j} - 1}{2} \frac{1}{tan\gamma_{z_j}} = 577.35$. The paths of the two aircraft during the simulation and the relative position of Aircraft 2 with respect

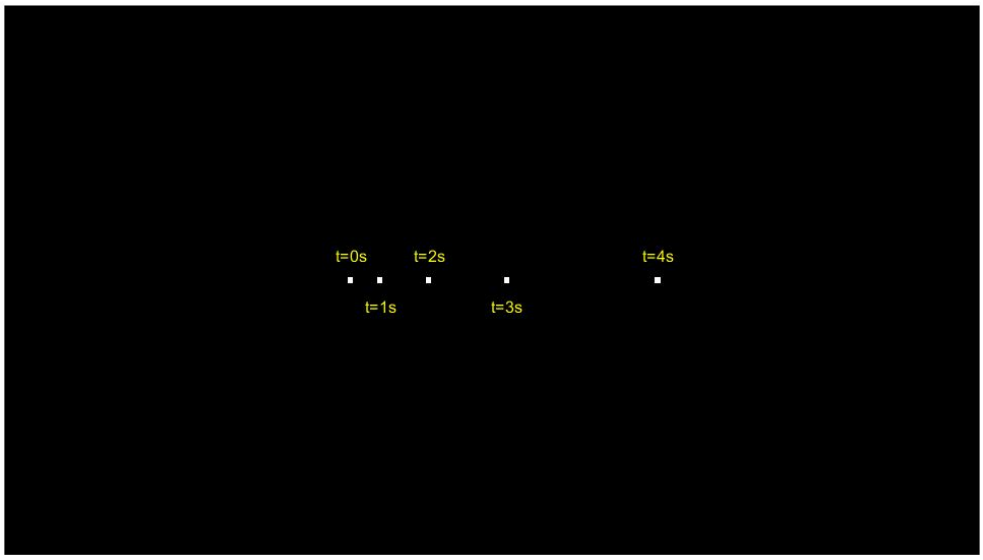

Figure 2.17. Case 3: Intruder Aircraft Right Camera Image.

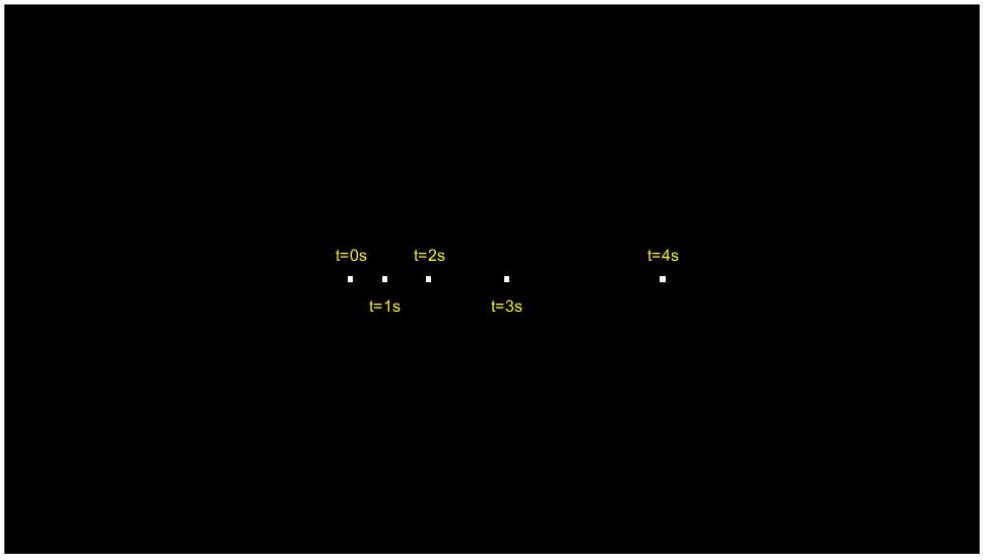

Figure 2.18. Case 3: Intruder Aircraft Left Camera Image.

Figure 2.19. Case 4: Intruder Aircraft Right Camera Image.

Figure 2.20. Case 4: Intruder Aircraft Left Camera Image.

to Aircraft 1 in terms of the three components in B_1-frame are shown in Fig. 2.11 and 2.12 respectively. The resulting camera images procured of Aircraft 2 in their respective C_j-frame are shown in Fig. 2.21 and 2.22. As one can observe, the images are virtually identical to the ones procured in Case 2.

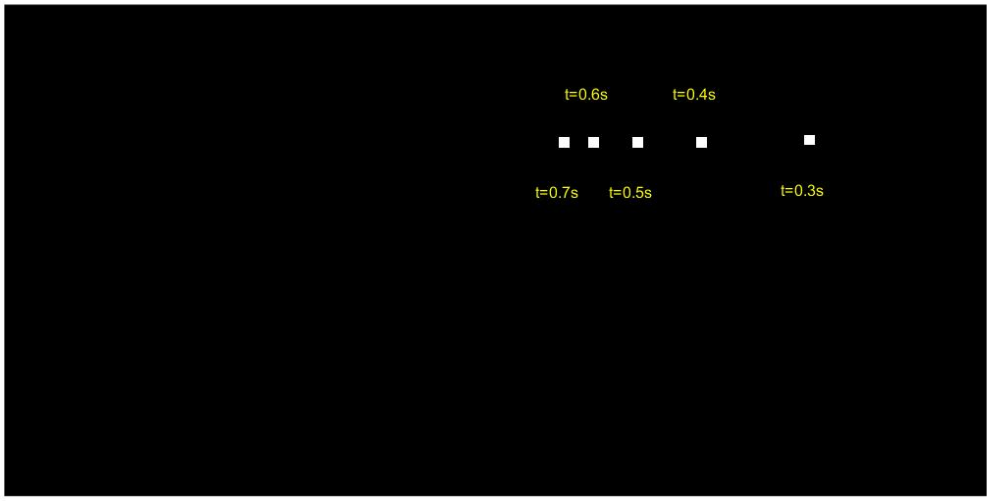

Figure 2.21. Case 5: Intruder Aircraft Right Camera Image.

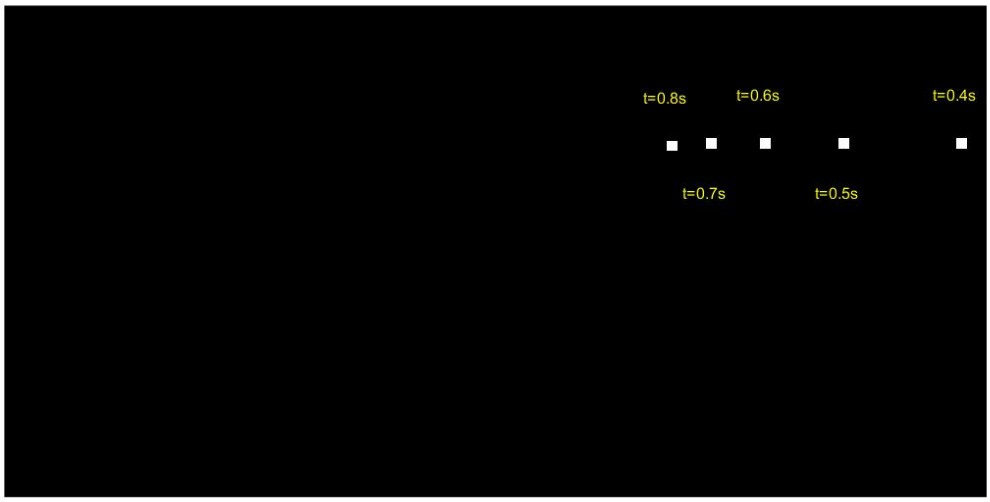

Figure 2.22. Case 5: Intruder Aircraft Left Camera Image.

CHAPTER 3

Relative Position Calculation

In the previous chapter, camera image(s) were generated of an intruder aircraft relative to an observer aircraft. This chapter now focuses on the 'reverse-engineering' part, which focuses on whether one could find the relative position of the intruder aircraft relative to the observer aircraft, assuming all that are given are the camera position(s) and orientation(s) relative to B_1-frame and the images taken by at least two cameras at the same times. This chapter will show two methods to finding the positions and test the veracity of each method using the same simulation test cases as those of Chapter 2. Both methods employ the epipolar geometry of stereo vision, based on two cameras view of 3D scene from two different positions. Both cameras are placed along a line parallel to the y-axis of B_1-frame, separated by a distance of b and both camera frames are aligned with B_1-frame.

3.1 Formulation

This section primarily focuses on the formulas required to attain the intruder aircraft position. The first method involves the use of trigonometry and triangular angles to obtain the answers, while the second method derives a general formulation based on the relation of actual positions and the distances on the virtual image frame.

3.1.1 Method 1 to Finding Position: Triangular Angles

This method involves using a combination of trigonometry and right-angled triangles to solve for the intruder aircraft position by first solving it relative to the

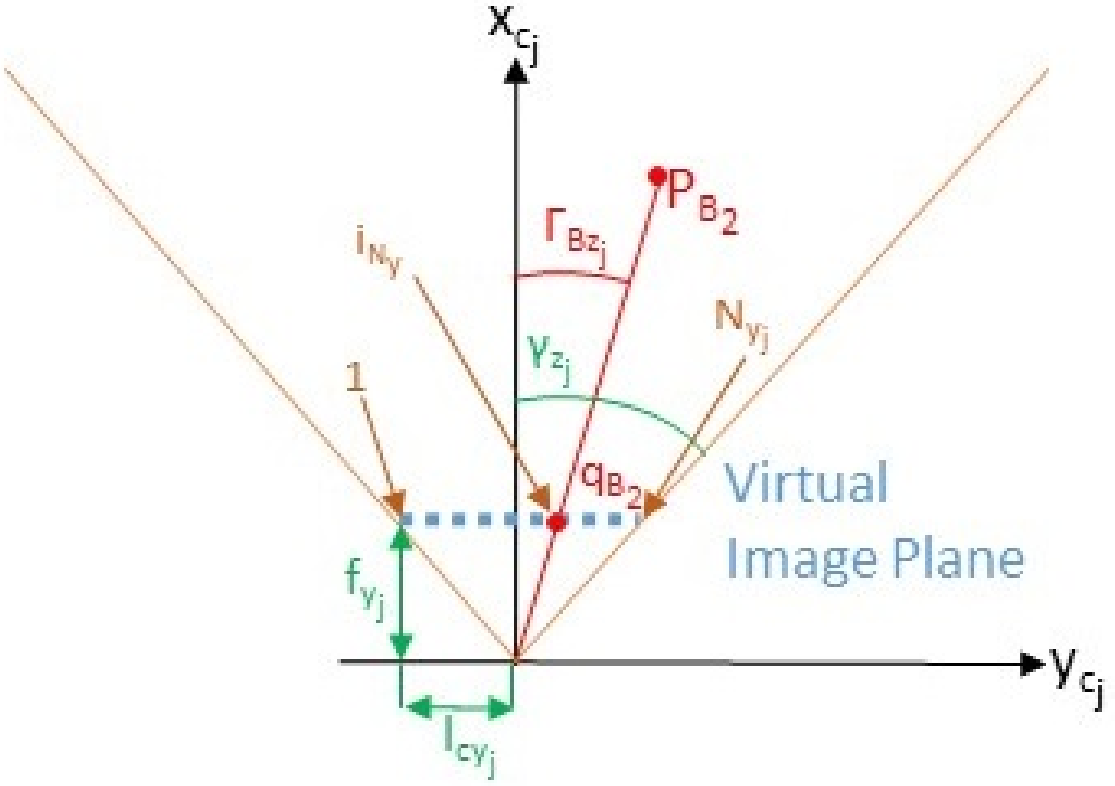

Figure 3.1. Angle of view and line of sight angle.

left camera, and then, through vector addition, solve for the position relative to the B_1-frame.

This method starts with determining $\gamma_{B_{z_j}}$, the line of sight angle from the camera-j to the intruder aircraft position; point p_{B_2}, as depicted in Fig. 3.1. Note that along the y_{C_j}-axis, there are N_{y_j} number of pixels and index i_{N_y} indicates the pixel of point q_{B_2}, the position of intruder aircraft image on the virtual image plane. Note also that $i_{N_y} = 1$ when $\gamma_{B_{z_j}} = -\gamma_{z_j}$ and $i_{N_y} = N_{y_j}$ when $\gamma_{B_{z_j}} = \gamma_{z_j}$. These two points are used to establish the linear relation between index i_{N_y} and γ_{z_j}, the line of sight angle as:

$$\Gamma_{Bz_j} = \frac{\gamma_{z_j}}{N_{y_j} - 1}(2i_{N_y} - N_{y_j} - 1) \tag{3.1}$$

Similarly, the line of sight angle in $(x_{C_j} - z_{C_j})$ plane is computed from the index along z_{C_j}-axis of the virtual image frame as:

$$\Gamma_{By_j} = \frac{\gamma_{y_j}}{N_{z_j} - 1}(2i_{N_z} - N_{z_j} - 1) \tag{3.2}$$

With the ling of sight angles computed, this method formulates the solution in five cases depending on the signs of the line of sight angles.

3.1.1.1 Case A: $\Gamma_{Bz_2} > 0$ and $\Gamma_{Bz_1} > 0$

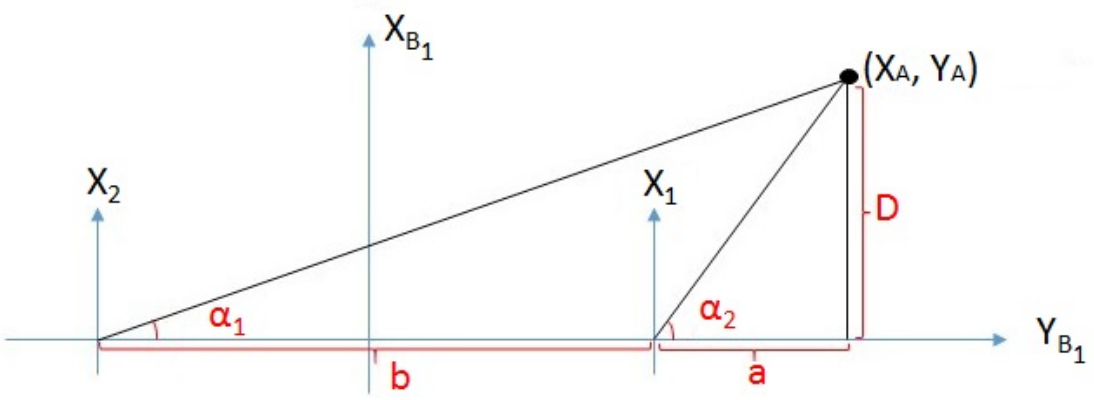

Figure 3.2. Triangular Angles Method: Case A.

In this case, the aircraft is located to the right of both cameras, as shown in Fig. 3.2. The angles are solved using the equations:

$$\alpha_1 = 90 - \Gamma_{Bz_1} \tag{3.3}$$

$$\alpha_2 = 90 - \Gamma_{Bz_2} \tag{3.4}$$

Using trigonometry, one gets the following equations for x and y positions relative to camera 2:

$$a = \frac{btan\alpha_2}{tan\alpha_1 - tan\alpha_2}$$

$$D = atan\alpha_1$$

$$x_{A_2} = D \tag{3.5}$$

$$y_{A_2} = a + b \tag{3.6}$$

Solving for the x and y intruder aircraft position relative to the origin of B_1-frame:

$$x_A = x_{A_2} + \rho_{C_{2,x}} \tag{3.7}$$

$$y_A = y_{A_2} + \rho_{C_{2,y}} \tag{3.8}$$

3.1.1.2 Case B: $\Gamma_{Bz_2} > 0$ and $\Gamma_{Bz_1} < 0$

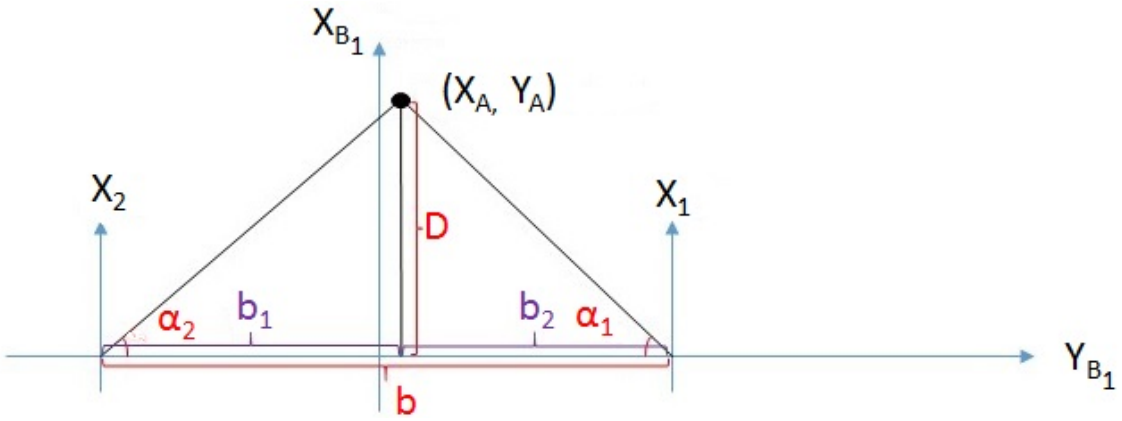

Figure 3.3. Triangular Angles Method: Case B.

In this case, the aircraft is located in between the two cameras, as shown in Fig. 3.3. The angles are solved using the equations:

$$\alpha_1 = 90 + \Gamma_{Bz_1} \tag{3.9}$$

$$\alpha_2 = 90 - \Gamma_{Bz_2} \tag{3.10}$$

Using trigonometry, one gets the following equations for x and y positions relative to camera 2:

$$b_2 = \frac{b}{1 + \frac{tan\alpha_2}{tan\alpha_1}}$$

$$D = b_2 tan\alpha_2$$

$$x_{A_2} = D \tag{3.11}$$

$$y_{A_2} = b_2 \tag{3.12}$$

Solving for the x and y intruder aircraft position relative to the origin of B_1-frame:

$$x_A = x_{A_2} + \rho_{C_{2,x}} \tag{3.13}$$

$$y_A = y_{A_2} + \rho_{C_{2,y}} \tag{3.14}$$

3.1.1.3 Case C: $\Gamma_{Bz_2} < 0$ and $\Gamma_{Bz_1} < 0$

In this case, the aircraft is located to the left of both the cameras, as shown in Fig. 3.4. The angles are solved using the equations:

$$\alpha_1 = 90 + \Gamma_{Bz_1} \tag{3.15}$$

$$\alpha_2 = 90 + \Gamma_{Bz_2} \tag{3.16}$$

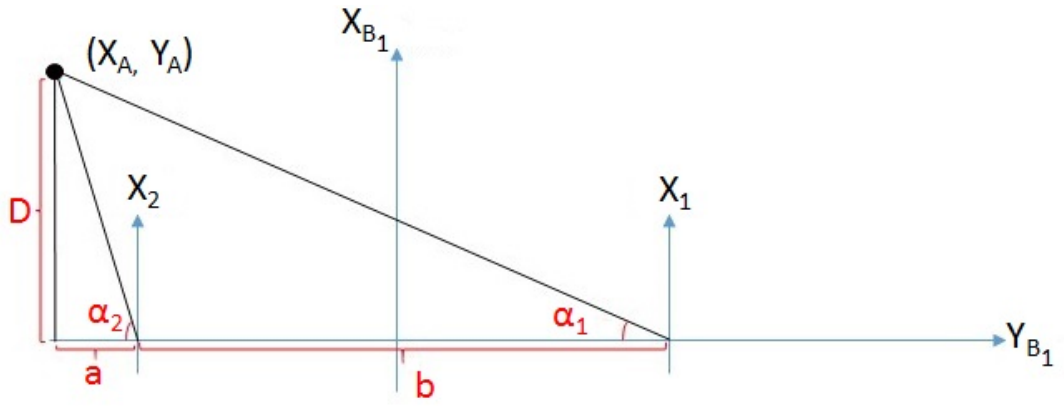

Figure 3.4. Triangular Angles Method: Case C.

Using trigonometry, one gets the following equations for x and y positions relative to camera 2:

$$a = -\frac{btan\alpha_2}{tan\alpha_1 - tan\alpha_2}$$

$$D = -atan\alpha_2$$

$$x_{A_2} = D \tag{3.17}$$

$$y_{A_2} = a \tag{3.18}$$

Solving for the x and y intruder aircraft position relative to the origin of B_1-frame:

$$x_A = x_{A_2} + \rho_{C_{2,x}} \tag{3.19}$$

$$y_A = y_{A_2} + \rho_{C_{2,y}} \tag{3.20}$$

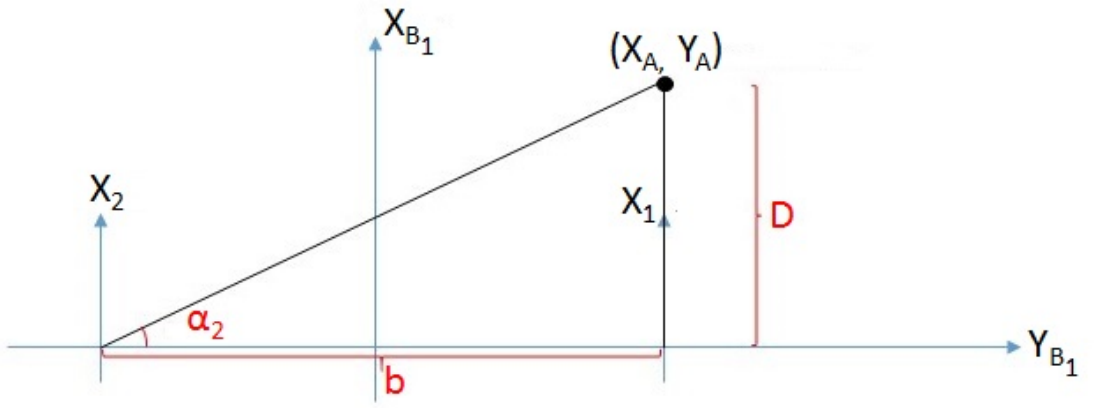

Figure 3.5. Triangular Angles Method: Case D.

3.1.1.4 Case D: $\Gamma_{Bz_2} > 0$ and $\Gamma_{Bz_1} = 0$

In this case, the aircraft is located at the center of Camera 1 and to the right of Camera 2, as shown in Fig. 3.5. The angles are solved using the equations:

$$\alpha_1 = 90 \tag{3.21}$$

$$\alpha_2 = 90 - \Gamma_{Bz_1} \tag{3.22}$$

Using trigonometry, one gets the following equations for x and y positions relative to camera 2:

$$D = b tan \alpha_2$$

$$x_{A_2} = D \tag{3.23}$$

$$y_{A_2} = b \tag{3.24}$$

Solving for the x and y intruder aircraft position relative to the origin of B_1-frame:

$$x_A = x_{A_2} + \rho_{C_{2,x}} \tag{3.25}$$

$$y_A = y_{A_2} + \rho_{C_{2,y}} \tag{3.26}$$

3.1.1.5 Case E: $\Gamma_{Bz_2} = 0$ and $\Gamma_{Bz_1} < 0$

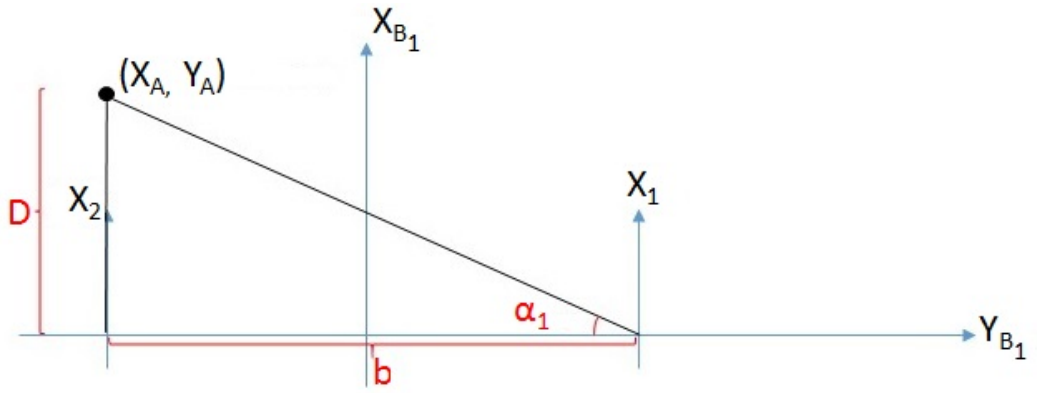

Figure 3.6. Triangular Angles Method: Case E.

In this case, the aircraft is located at the center of Camera 2 and to the left of Camera 2, as shown in Fig. 3.6. The angles are solved using the equations:

$$\alpha_1 = 90 + \Gamma_{Bz_1} \tag{3.27}$$

$$\alpha_2 = 90 \tag{3.28}$$

Using trigonometry, one gets the following equations for x and y positions relative to camera 2:

$$D = btan\alpha_1$$

$$x_{A_2} = D \tag{3.29}$$

$$y_{A_2} = 0 \tag{3.30}$$

Solving for the x and y intruder aircraft position relative to the origin of B_1-frame:

$$x_A = x_{A_2} + \rho_{C_{2,x}} \tag{3.31}$$

$$y_A = y_{A_2} + \rho_{C_{2,y}} \tag{3.32}$$

3.1.1.6 Solving for Aircraft Position z_A

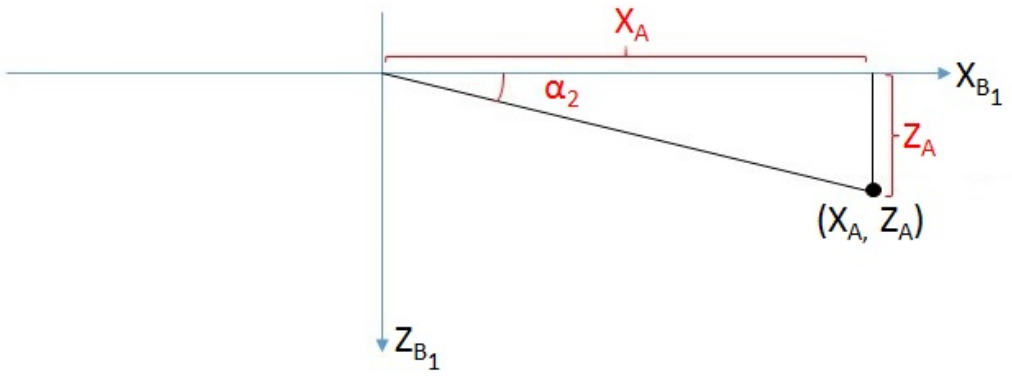

Figure 3.7. Triangular Angles Method: z_A Calculation.

Now that x_A and y_A have been solved, the next step is to solve for z_A. Since the cameras are only translated along the y-direction (the x and z positions are the same for both), the z_A position can be easily calculated. As one can observe on Fig. 3.7, all one needs are the values of x_A and the angle α_2, which is:

$$\alpha_2 = \Gamma_{By_2} \tag{3.33}$$

The intruder aircraft's z-position in the Camera 2 frame is:

$$z_{A_2} = x_{A_2} tan\alpha_2 \tag{3.34}$$

This in turn gives the intruder aircraft's z-position relative to the origin of B_1-frame to be:

$$z_A = z_{A_2} + \rho_{C_{2,z}} \tag{3.35}$$

3.1.2 Method 2 to Finding Position: Virtual Image Frame Utilization

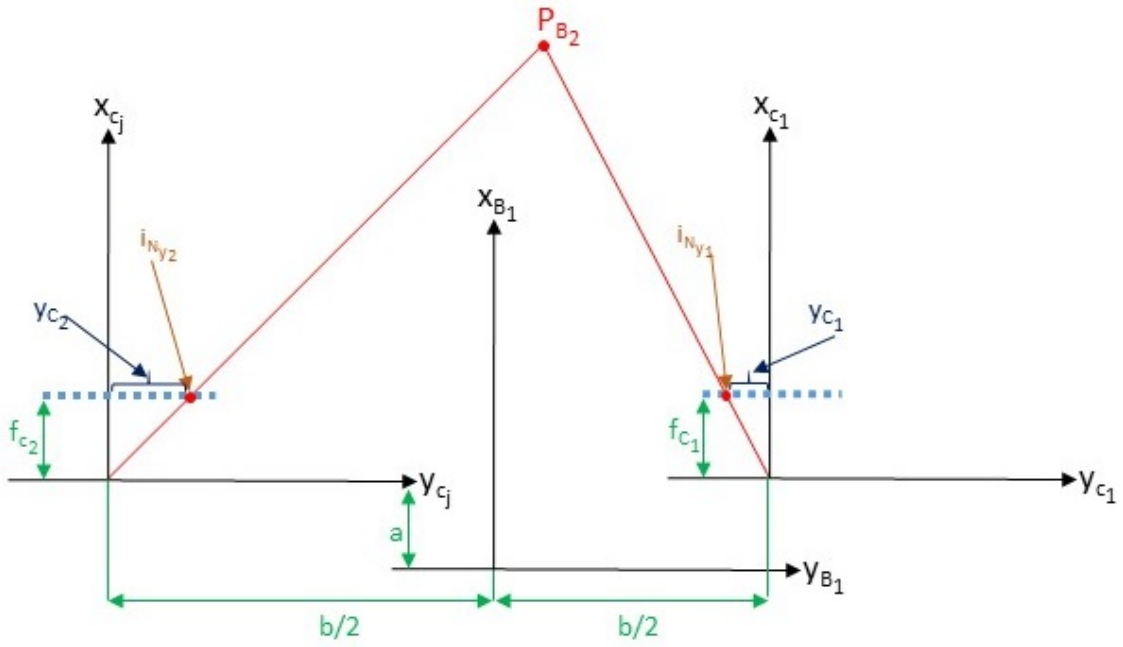

Figure 3.8. Epipolar Geometry of two cameras.

Fig. 3.8 depicts the epipolar geometry of the two cameras and introduces the quantities used in the following formulations. Note that these quantities directly

follow the notation introduced in Chapter 2. Consider that the two camera positions are placed in the B_1-frame as:

$$\rho_{C_1} = \begin{bmatrix} a \\ b/2 \\ c \end{bmatrix} \qquad and \qquad \rho_{C_2} = \begin{bmatrix} a \\ -b/2 \\ c \end{bmatrix} \tag{3.36}$$

Cameras 1 and 2 have focal lengths of f_{C_1} and f_{C_2}, respectively. At a specific time, the intruder aircraft, Aircraft 2 is located at point p_{B_2} and visible in both cameras. Consider indices $(i_{N_{z_1}}, i_{N_{y_1}})$ and $(i_{N_{z_2}}, i_{N_{y_2}})$ indicating the position of the pixels that correspond projections of point p_{B_2} on virtual image frames of Camera 1 and 2, respectively. The position of p_{B_2} relative to B_1-frame is

$$\xi = \begin{bmatrix} x_A \\ y_A \\ z_A \end{bmatrix} \tag{3.37}$$

The problem can now be defined as to find (x_A, y_A, z_A) given indices $(i_{N_{z_1}}, i_{N_{y_1}})$ and $(i_{N_{z_2}}, i_{N_{y_2}})$.

Using Eqs. (2.22) and (2.23) in Chapter 2,

$$i_{y_j} = 100[\frac{2(i_{N_{y_j}} - 1)}{N_{y_j} - 1} - 1] \tag{3.38}$$

$$i_{z_j} = 100[\frac{2(i_{N_{z_j}} - 1)}{N_{z_j} - 1} - 1] \tag{3.39}$$

where $j = \{1, 2\}$. Using the indices, Eqs. (2.18) and (2.19) can be solved for the pixel positions in the virtual image frames as:

$$y_{C_j} = \frac{1}{100} i_{y_j} l_{Cy_j} \tag{3.40}$$

$$z_{C_j} = \frac{1}{100} i_{z_j} l_{Cz_j} \tag{3.41}$$

where l_{Cy_j} and l_{Cz_j} are half-lengths of the image frames in y and z-axes, respectively, and can be computed from the focal lengths and view angles formulated in Eqs. (2.10) and (2.11).

Putting all these equations together yield:

$$y_{C_j} = [\frac{2(i_{N_{y_j}} - 1)}{N_{y_j} - 1} - 1] f_{C_j} tan\gamma_{z_j} \tag{3.42}$$

$$z_{C_j} = [\frac{2(i_{N_{z_j}} - 1)}{N_{z_j} - 1} - 1] f_{C_j} tan\gamma_{y_j} \tag{3.43}$$

where $j = \{1, 2\}$ and also note that these equations depend on camera parameters: f_{C_j}, the focal length; γ_{z_j} and γ_{y_j}, the angles of view in $x_{C_j} - y_{C_j}$ and $x_{C_j} - z_{C_j}$ planes, respectively; and N_{y_j} and N_{z_j}, the number of pixels along the y_{C_j} and z_{C_j} directions, respectively. These sets of parameters are related as:

$$f_{C_j} = \frac{(N_{y_j} - 1)}{2} \frac{1}{tan\gamma_{z_j}} \tag{3.44}$$

$$f_{C_j} = \frac{(N_{z_j} - 1)}{2} \frac{1}{tan\gamma_{y_j}} \tag{3.45}$$

Let us define the position p_{B_2} in Fig. 3.8 in each camera frame:

$$\xi_{C_j} = \begin{bmatrix} x_{A_j} \\ y_{A_j} \\ z_{A_j} \end{bmatrix}, \qquad j = \{1, 2\} \tag{3.46}$$

Since the camera frames are aligned with B_1-frame,

$$\xi_{C_j} = \xi - \rho_{C_j}, \qquad j = \{1, 2\} \tag{3.47}$$

which along with Eqs. (3.36), (3.37) and (3.46) imply

$$\begin{aligned} x_{A_j} &= x_A - a, && j = \{1,2\} \\ y_{A_1} &= y_A - \frac{b}{2} \\ y_{A_2} &= y_A + \frac{b}{2} \\ z_{A_j} &= z_A - c, && j = \{1,2\} \end{aligned} \tag{3.48}$$

Using the properties of similar triangles, as depicted in Fig. 3.8 leads to

$$\frac{y_{C_j}}{f_{C_j}} = \frac{y_{A_j}}{x_{A_j}}$$
$$\frac{z_{C_j}}{f_{C_j}} = \frac{z_{A_j}}{x_{A_j}}$$

Substituting x_{A_j}, y_{A_j}, and z_{A_j} from Eq. (3.48) in these equations yield

$$\frac{y_{C_1}}{f_{C_1}} = \frac{y_A - \frac{b}{2}}{x_A - a} \tag{3.49}$$

$$\frac{y_{C_2}}{f_{C_2}} = \frac{y_A + \frac{b}{2}}{x_A - a} \tag{3.50}$$

$$\frac{z_{C_1}}{f_{C_1}} = \frac{z_{C_2}}{f_{C_2}} = \frac{z_A - c}{x_A - a} \tag{3.51}$$

Eqs. (3.49) and (3.50) imply

$$x_A - a = \frac{f_{C_1}}{y_{C_1}}(y_A - \frac{b}{2}) \tag{3.52}$$

$$x_A - a = \frac{f_{C_2}}{y_{C_2}}(y_A + \frac{b}{2}) \tag{3.53}$$

which imply

$$\frac{f_{C_1}}{y_{C_1}}(y_A - \frac{b}{2}) = \frac{f_{C_2}}{y_{C_2}}(y_A + \frac{b}{2})$$

which is solved for its only unknown as

$$y_A = \frac{b}{2}(\frac{f_{C_1}y_{C_2} + f_{C_2}y_{C_1}}{f_{C_1}y_{C_2} - f_{C_2}y_{C_1}})$$

Once y_A is calculated by this equation, Eqs. (3.52) or (3.53) is used to compute x_A:

$$x_A = \frac{f_{C_1}}{y_{C_1}}(y_A - \frac{b}{2}) + a \tag{3.54}$$

$$x_A = \frac{f_{C_2}}{y_{C_2}}(y_A + \frac{b}{2}) + a \tag{3.55}$$

Note that these equations experience division by zero when y_{C_1} or y_{C_2} is zero. Since y_{C_1} or y_{C_2} cannot both be zero at the same time, the other equation should be used to compute x_A when one of either y_{C_1} or y_{C_2} is zero.

Finally, with x_A calculated, Eq. (3.51) is used to compute z_A as:

$$z_A = \frac{z_{C_j}}{y_{C_j}}(x_A - a) + c, \qquad j = \{1, 2\}$$

which should give the same result for both $j = 1$ and $j = 2$.

3.2 Simulation Results

This section simulate the same four cases introduced in Chapter 2. In Chapter 2, the camera images are generated. In this section, the relative position of the intruder aircraft with respect to the observer aircraft is calculated based on the camera images only. Relative position calculation is repeated for the two methods introduced above. The results are presented below to show the performance of both methods in estimating the relative position.

3.2.1 Case 1

Case 1 is the simplest case, involving the observer and intruder aircraft travelling parallel to each other and the intruder flying faster than the observer. The calculated x, y, and z positions over time are shown in Fig. 3.9 and the distances between the two aircraft over time are shown in Fig. 3.10.

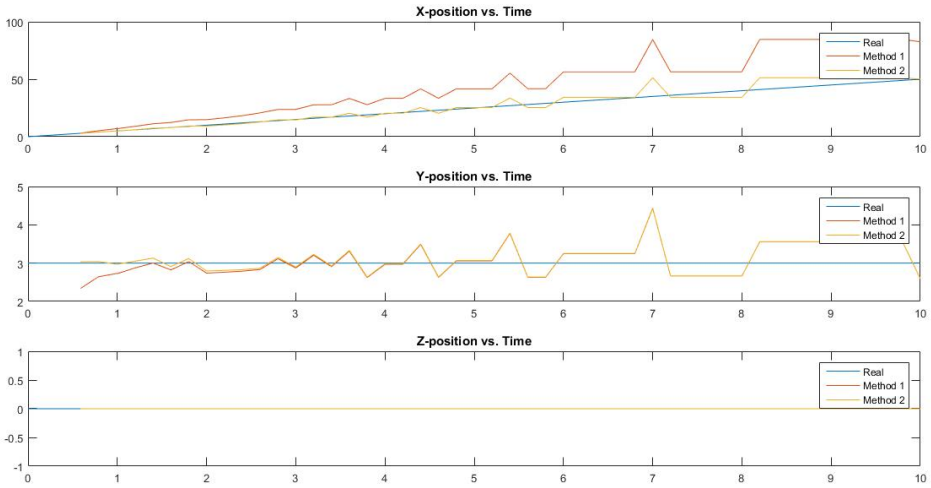

Figure 3.9. Case 1 Results: Calculated Position Values.

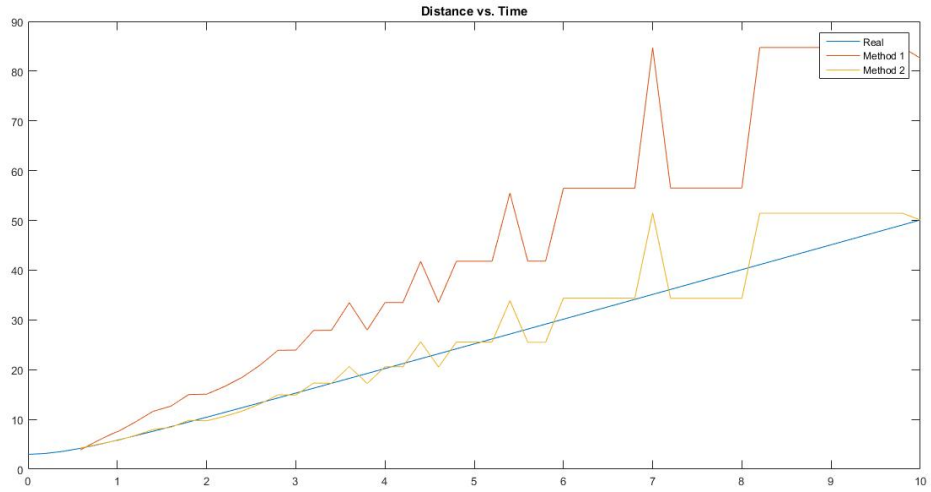

Figure 3.10. Case 1 Results: Calculated Distance Values.

3.2.2 Case 2

Case 2 involves the observer aircraft maintaining level flight, and the intruder aircraft yaw and pitch at -1 deg and 1 deg, respectively. The calculated x, y, and z

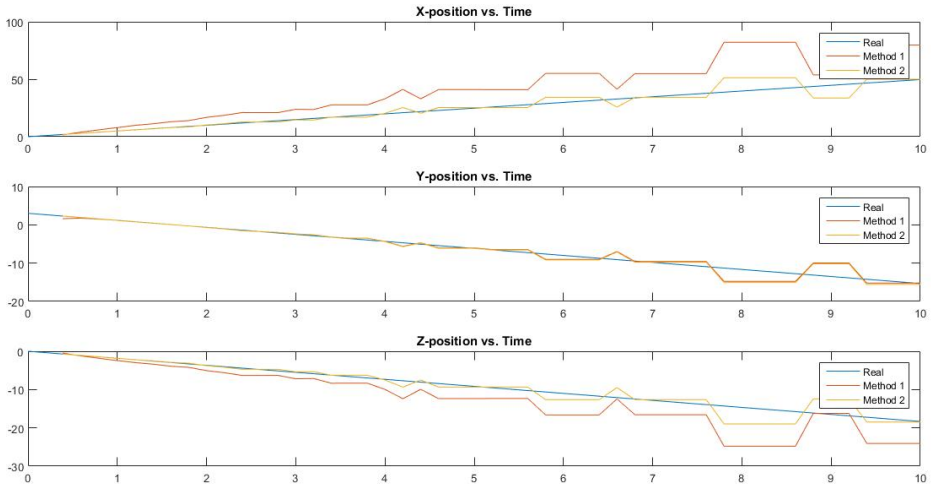

Figure 3.11. Case 2 Results: Calculated Position Values.

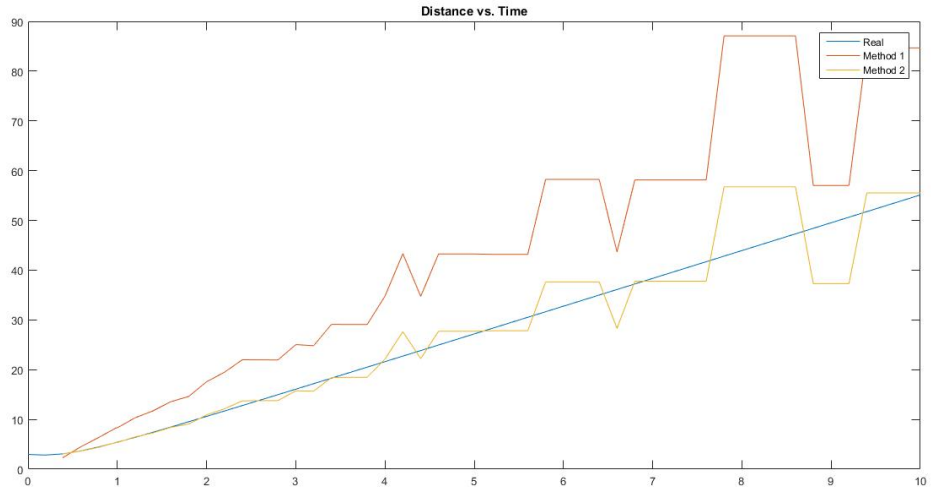

Figure 3.12. Case 2 Results: Calculated Distance Values.

positions over time are shown in Fig. 3.11 and the distances between the two aircraft over time are shown in Fig. 3.12.

3.2.3 Case 3

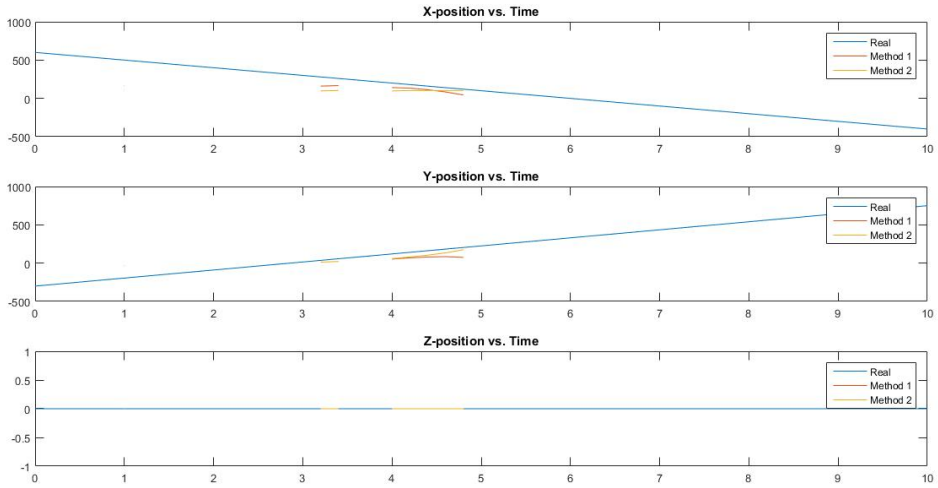

Figure 3.13. Case 3 Results: Calculated Position Values.

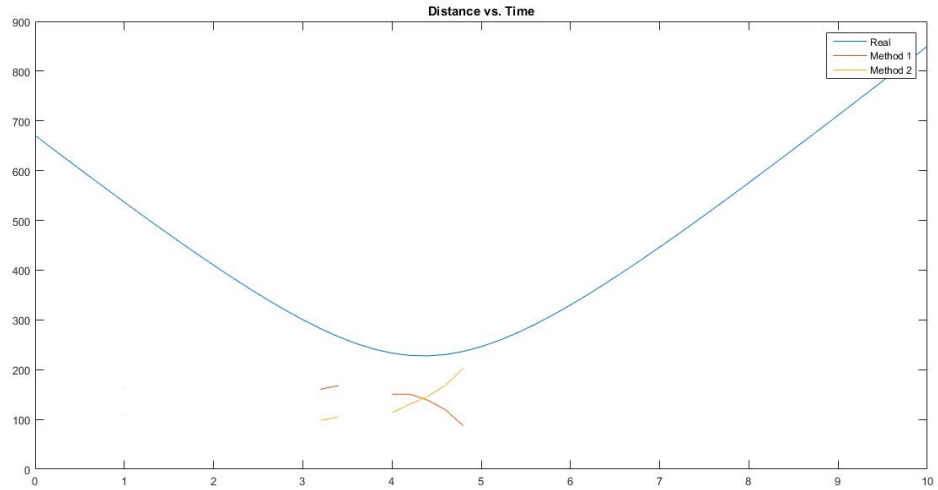

Figure 3.14. Case 3 Results: Calculated Distance Values.

Case 3 involves both the intruder and the observer aircraft fly perpendicular to each other. The calculated x, y, and z positions over time are shown in Fig. 3.13 and the distances between the two aircraft over time are shown in Fig. 3.14. If one observes the images carefully, it can be seen that there are disjointed intervals when performing position calculation. This is because the disparity (the difference between the column indices where the aircraft is visible on each camera) is 0, which in turn means that the aircraft is too far away to calculate the relative position.

3.2.4 Case 4

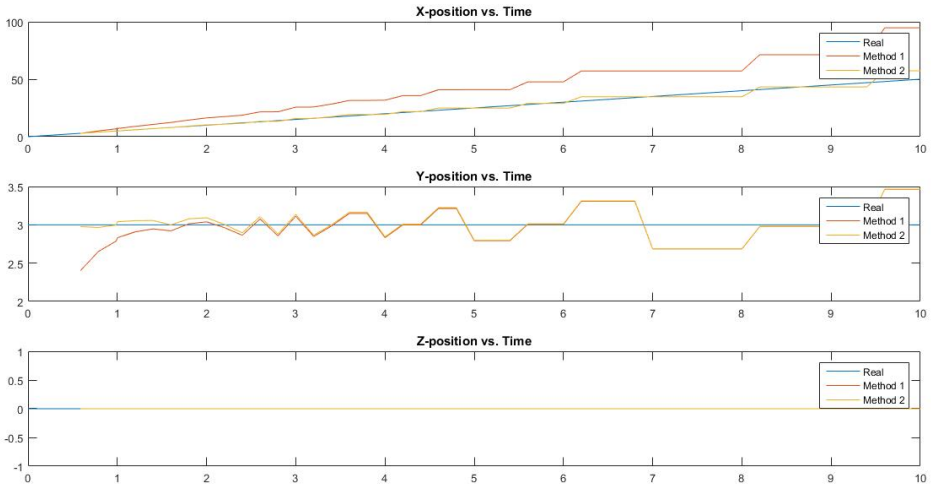

Figure 3.15. Case 4 Results: Calculated Position Values.

Case 4 is a repeat of Case 1, but with increased separation between the 2 cameras. The calculated x, y, and z positions over time are shown in Fig. 3.15 and the distances between the two aircraft over time are shown in Fig. 3.16.

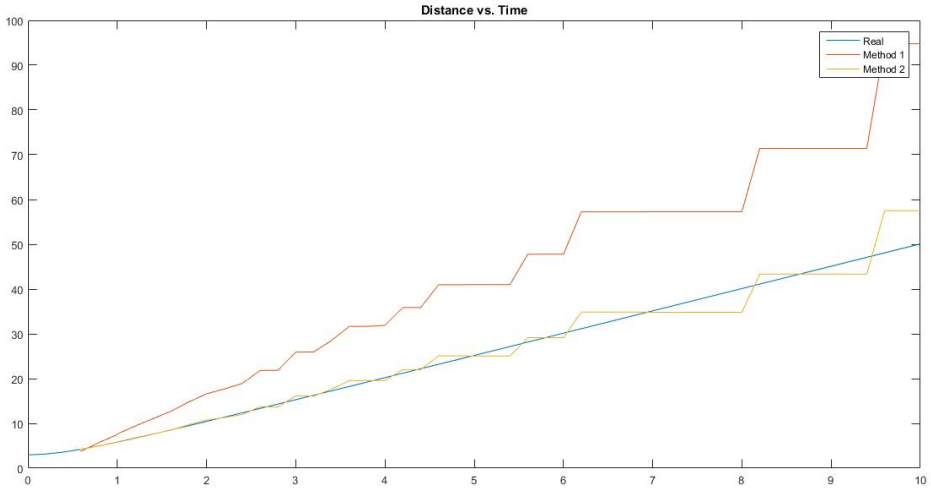

Figure 3.16. Case 4 Results: Calculated Distance Values.

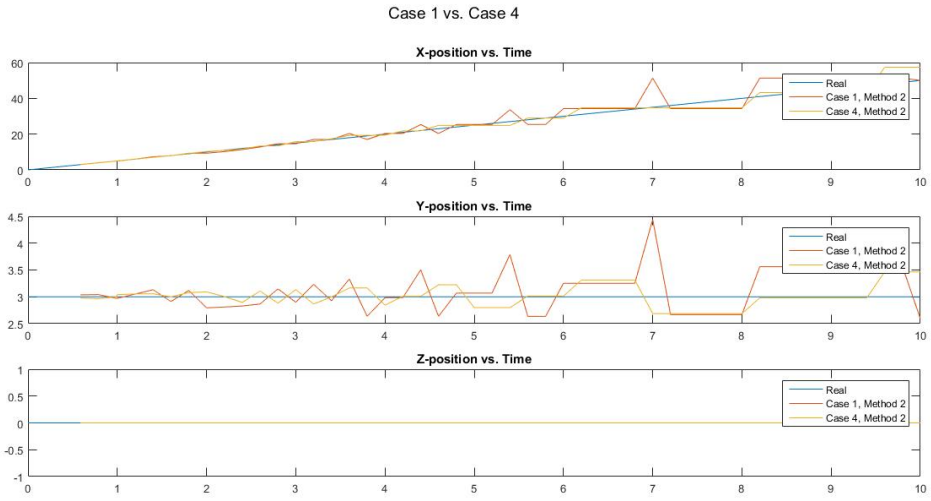

Figure 3.17. Case 1 vs. Case 4 - Calculated Position Values.

When observing the plots obtained here to those of Case 1 (Figs. 3.9 and 3.10), it can be observed that Case 4 more accurately measures the position of the aircraft than Case 1 does at the same point. This can be further be confirmed using Fig.

3.17,where both the plots obtained using the second method 'follow' the actual line when the distances are closer, but only Case 4 manages to maintain that trajectory somewhat when distance between the aircraft increase.

3.2.5 Case 5

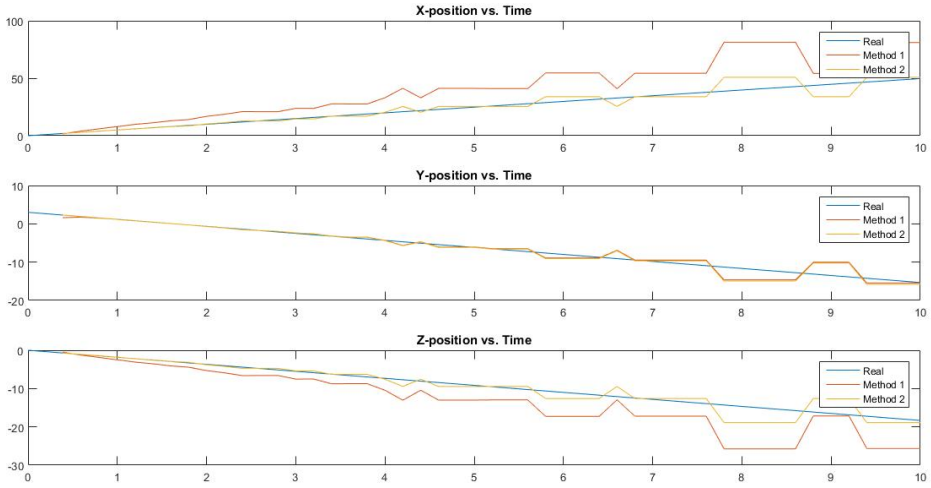

Figure 3.18. Case 5 Results: Calculated Position Values.

Case 5 is a repeat of Case 2, but with lowered image resolution. The calculated x, y, and z positions over time are shown in Fig. 3.18 and the distances between the two aircraft over time are shown in Fig. 3.19.

When observing the plots obtained here to those of Case 2 (Figs. 3.11 and 3.12), it can be observed that Case 5 and Case 2 provide virtually identical results, with Case 5 being only marginally worse than Case 2 with larger distances. This can be further be confirmed using Fig. 3.20, where both the plots obtained using the

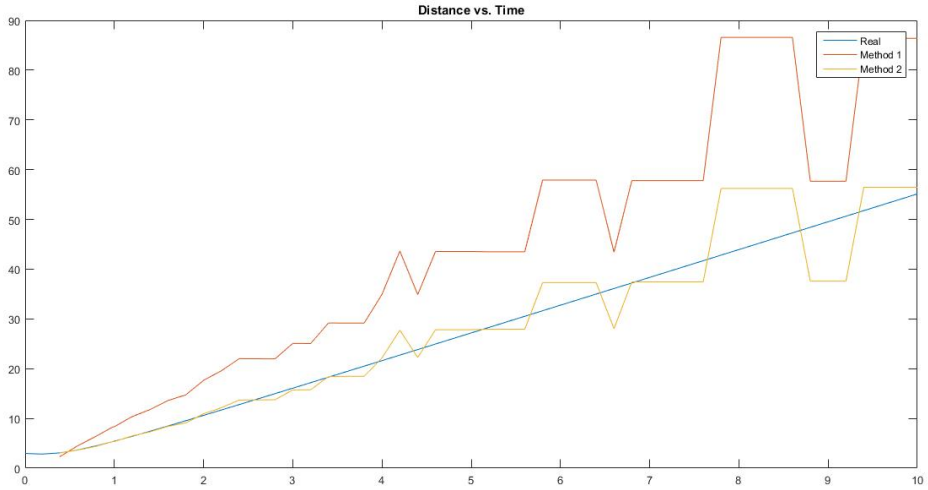

Figure 3.19. Case 5 Results: Calculated Distance Values.

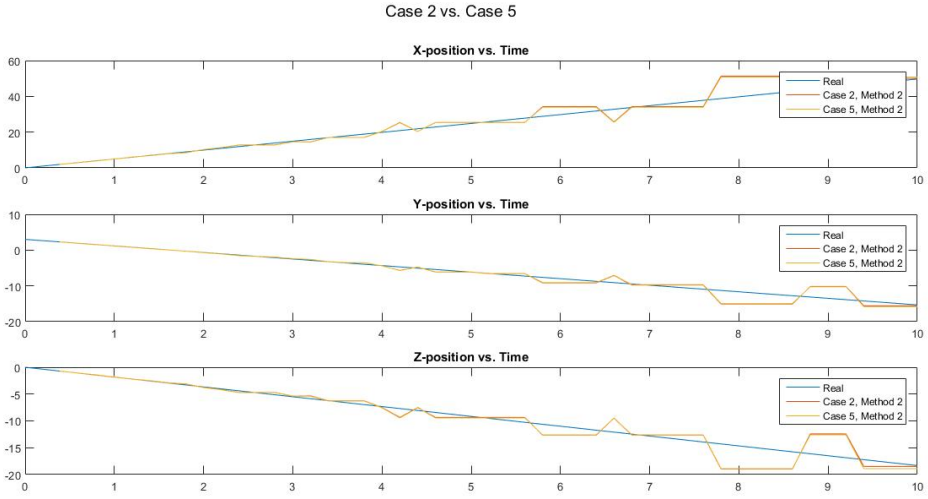

Figure 3.20. Case 2 vs. Case 5 - Calculated Position Values.

second method 'follow' the actual line, although the difference between the is slightly more evident as position values get larger.

3.2.6 Case Results Summary

When observing the above five cases, there are a few key observations one can make:

- Both of the methods above give similar results, although the focal length method (Method 2) is more accurate as the plot 'follows' the real simulated values, while the values obtained on Method 1 veer away from the real simulated values with increasing distance.
- As the distance between the 2 aircraft increase, the accuracy of the results obtained decrease. The accuracy is virtually non-existent if they are too far, as demonstrated in Case 3.
- The accuracy of the result is also dependent on the baseline length. The larger the baseline length, the more accurate the calculation.
- The image resolution has negligible impact on the accuracy of the results obtained.
- When distance increases, there are occurrences where the estimated position stay constant while the actual position increases. This is due to the fact that as the aircraft travels farther and farther away, the disparity between image points decrease. In fact, it is precisely because of this that the position estimation accuracy deteriorates with increasing distance.

These results suggest that the methods used do provide useful results as long as the observer aircraft is reasonably close to the intruder aircraft.

CHAPTER 4

Conclusion and Future Work

The overall focus of this chapter is to summarize the results of this research and suggest methods with which the results could be improved.

4.1 Conclusion

First, rotational and translational kinematics equations were introduced; these were used to develop various flight simulations which allowed one to determine the position of the intruder aircraft relative to the observer aircraft. After this step was completed, equations were developed which allowed one to map the position of the aircraft relative to 2 cameras placed in pre-determined locations on the observer aircraft.

Using the images (and the camera location and viewing angles which were known in advance), 2 different methods were developed which allowed one to 'reverse-engineer' (i.e., find the position of the intruder aircraft relative to the observer). The calculated results were then compared to the results obtained from the kinematics equations to determine the degree of accuracy with which either method determined the intruder aircraft position. Overall, it was determined that it is indeed possible to estimate the relative position while both aircraft are flying along any trajectories as long as the intruder aircraft is visible by both cameras. It was also determined that the second method - which utilized the virtual image frame - provided more accurate estimation results. Both calculation methods did, however, share several common traits: (i) The estimation accuracy degraded as the relative distance increased be-

tween the aircraft (ii) The larger lateral separation seemed to improve the estimation accuracy, and (iii) Image resolution seemed to have little to no impact on estimation accuracy.

4.2 Future Work

Some of the ways with which distance calculation could be improved in the future include:

- Instead of creating binary matrices to simulate image processing, use actual images of intruder aircraft (taken by an observer aircraft) and perform the algorithm directly
- Use stereo cameras that do not follow the simple stereo camera setup (i.e., cameras that are both rotated and translated at various orientations relative to each other as opposed to simple translation along y-axis without any rotation)
- Test the veracity of the algorithm used for ever increasingly complex flight cases.

These methods should help not only in increasing the various possible ways with which one can solve for the positions, but it should also increase the accuracy of the results obtained.

REFERENCES

[1] W. Paper, "Understanding compliance with automatic dependent surveillance broadcast (ads-b) out," *Universal Avionics Systems Corporation*, February 2014.

[2] T. Z. A. Z. B. V. T. P. J. B. T. Roska, "Collision avoidance for uav using visual detection," *2011 IEEE International Symposium of Circuits and Systems (ISCAS)*, May 2011.

[3] A. Dogan and W. Blake, "Equations of motion - introduction," in *Flight Mechanics of Aerial Refueling:Mathematical Modeling and Simulation*, 2015.

[4] Wikipedia, "Pinhole camera model," Online. Available at https://en.wikipedia.org/wiki/Pinhole_camera_model. Accessed 28-April-2016.

[5] J. Mrovlje and D. Vrancic, "Distance measuring based on stereoscopic pictures," in *9th International PhD Workshop on Systems and Control: Young Generation Viewpoint*, October 2008.

BIOGRAPHICAL STATEMENT

Aditya Ramani was born in Chennai, Tamil Nadu, India in 1991. He received his Bachelors of Applied Science degree in Electrical Engineering from the University of Toronto in Toronto, Canada, in 2013. He is currently pursuing his Master's in Aerospace Engineering from the University of Texas at Arlington, with the focus of his research being on the Determination of Intruder Aircraft Position using Stereoscopic Images.